Interplay of MPP5a with Rab11 synergistically builds epithelial apical polarity and zonula adherens

Yumei Hao[1,2,6], Yao Zhou[1,2,6], Yinhui Yu[1,6], Mingjie Zheng[1,2], Kechao Weng[1,2], Ziqi Kou[1,2], Jiancheng Liang[1,2], Qian Zhang[3], Xiajing Tang[1], Pinglong Xu[3], Brian A. Link[4], Ke Yao[1,5*], Jian Zou[1,2,5,*]

[1]Eye Center of the Second Affiliated Hospital, School of Medicine, Zhejiang University, Hangzhou, 310058, China

[2]The Institute of Translational Medicine, Zhejiang University, Hangzhou, 310058, China

[3]Life Sciences Institute and Innovation Center for Cell Signaling Network, Zhejiang University, Hangzhou, 310058, China

[4]Department of Cell Biology, Neurobiology and Anatomy, Medical College of Wisconsin, Milwaukee, Wisconsin 53226, USA

[5]Zhejiang Provincial Key Lab of Ophthalmology, Hangzhou, 310058, China

[6]These authors contribute equally

[*] Correspondence: jianzou@zju.edu.cn; xlren@zju.edu.cn

Summary statement

The key apical polarity protein MPP5a interplays with small GTPase Rab11 to synergistically guide the apical polarization and zonula adherens formation in epithelial cells.

ABSTRACT

Adherens junctions remodeling regulated by apical polarity proteins constitutes a major driving force for tissue morphogenesis, though the precise mechanism remains inconclusive. Here we reported that Crumbs complex component MPP5a interacts with small GTPase Rab11 in Golgi to synergistically transport cadherin and Crumbs components to the apical domain, thus establishing the apical epithelial polarity and adherens junctions. In contrast, Par complex recruited by MPP5a is incapable to interact with Rab11 but may assemble cytoskeleton to facilitate the cadherin exocytosis. In accordance, dysfunction of MPP5a induced an invasive migration of epithelial cells. This adherens junctions remodeling pattern is frequently observed in zebrafish lens epithelial cells and neuroepithelial cells. The data identified an unrecognized MPP5a/Rab11 complex and described its essential role in guiding the apical polarization and zonula adherens formation in epithelial cells.

Keywords: MPP5a; Rab11; apical polarity; adherens junctions remodeling; zonula adherens

INTRODUCTION

Adherens junctions (AJs) remodeling and cytoskeleton rearrangement are the major driving force of cell migration, which play essential roles in both organogenesis and diseases, such as convergent extension and collective cell migration. Adapting to cell state, AJs can be assembled into three diverse modes including punctum adherens, zonula adherens and tricellular adherens, depending on shape, position, and mode of actin filament association with AJs (Yonemura, 2011), which endowing the cells with dual properties of rigidity and plasticity (Harris and Tepass, 2010; Balda and Matter, 2016). For instance, the zonula adherens exist at the apical domain is the hallmark of epithelial cells and necessary to stabilize the epithelial tissue.

Remodeling of AJs involves both the activity of Rab family small GTPases and the role of cellular polarity proteins (Harris and Tepass, 2010; Bruser and Bogdan, 2017; Apodaca et al., 2012). Rab family proteins, which are known to control membrane identity and vesicle trafficking between organelles (Stenmark, 2009; Scott et al., 2014), participate in the recycling of AJs. Among these Rab proteins, Rab5 is crucial for the formation of the early endosome (Chavrier et al., 1990; Gorvel et al., 1991; Barbieri et al., 1996). The proteins internalized into early endosome are sorted either for degradation in the endolysosomal pathway or for recycling. Rab11 functions as a key regulator in the recycling endosomes and in the trans-Golgi network–to–plasma membrane transport, which is critical for establishing the apical zonula adherens in epithelial cells (Ullrich et al., 1996; Chen et al., 1998; Woichansky et al., 2016). However, the causation that Rab11 guides the vesicles specifically to the apical domains of cells is still not well understood, although a series of interacting proteins of Rab11 has previously been identified (Apodaca et al., 2012).

Rab11, the Rab family small GTPase and key trafficking regulator of AJs components, is associated with cellular polarity complex (Harris and Tepass, 2008; Roeth et al., 2009; Bryant et al., 2010; Clark et al., 2011; Sobajima et al., 2014; Hosono et al., 2015). Rab11 usually enriches at the apical domains in epithelial cells. The apical localization of Rab11 appears to need polarity proteins. For instance, aPKC, the key kinase in Par6-Par3-aPKC-CDC42 (Par) complex, modulates the

orientation of actomyosin cables to promote the Rab11-mediated exocytosis in the *Drosophila* (Harris and Tepass, 2008; Hosono et al., 2015), and non-apical polarity protein Par5 functions as a regulatory hub for Rab11-positive recycling endosomes in *C. elegans* (Winter et al., 2012). Nevertheless, the regulatory protein(s) that drive Rab11-mediated apical vesicle trafficking in vertebrates are still not identified.

The complexes of Crumbs-MPP5a-PATJ (Crb) and Par6-Par3-aPKC-CDC42 are the key determinants of epithelial apical polarity that function conservatively in multiple organs cross *Drosophila* to mammals (Bulgakova and Knust, 2009; Tepass, 2012; Chen and Zhang, 2013). Both the Crb complex and the Par complex are required for the AJs modeling in epithelial cells. Ablation of these complexes leads to the similar defects in the formation of apical zonula adherens (Tepass, 1996; Klebes and Knust, 2000; Joberty et al., 2000; Hurd et al., 2003; Omori and Malicki, 2006; van de Pavert et al., 2007; Park et al., 2011; Flores-Benitez and Knust 2015; Ramkumar et al., 2016). Functional interaction between Crb and Par complexes are well defined. MPP5a, one of the key components of the Crb complex, directly interacts with Par6 to recruit Par complex and facilities its aggregation at the apical domains of epithelial cells. On the other hand, aPKC phosphorylates the intracellular domain of Crb protein that resulting in the exchange of intracellular Crb partner from FERM-domain proteins to MPP5a, thus restricting the apical localization of Crb (Hurd et al., 2003; Sotillos et al., 2004; Penkert et al., 2004; Laprise et al., 2006; Hsu et al., 2006; Fletcher et al., 2012; Wei et al., 2015). Because of functional association, it is still inconclusive as to the precise mechanism and exact function of both complexes during the remodeling of AJs, although various phenotype defects of diverse organs have been reported upon their absence.

In this study, we aim to elucidate *in vivo* the coordinative mechanism to link epithelial membrane traffic, AJs remodeling, and apical polarity machineries during cell state transition in vertebrates. Using developing zebrafish lens and retina as models, we report here that MPP5a interacts with GTPase Rab11 to transport both Crb complex and AJs components to the apical domain, thus establishing the apical polarity. Therefore, dysfunction of either Crb complex or Rab11 causes the

failure in the apical transport of Crb components and undesired and instable punctum adherens, which leading to an invasive migration and cataract-like phenotype. On the other hand, Par complex may regulate cytoskeleton arrangement, but not directly interplay with the Rab11, to accommodate the vesicle transport.

RESULTS

AJs are dynamically remodeled during lens cell state transition

To investigate the mechanism of Crb complex involving in AJs assembly, we first examined in wild-type (WT) lens for the AJs remodeling pattern during cell state transition. The E-cadherin displayed non-polarized localization in lens epidermal cells at 24 hpf (hour post fertilization), and enriched at the vertex point where three neighbor cells meet (Fig. 1A and 1B). TEM observations revealed that tricellular adherens at the foci and punctum adherens between lateral membranes of epidermal cells constituted the major types of adhesion plaques in lens (Fig. 1C, 1D, and S1A-S1C). At 28 hpf when epidermal-to-epithelial transition occurred (Greiling et al., 2009), E-cadherin was gradually accumulated at the apical domains of epithelial cells in anterior lens (Fig. 1E and 1F). TEM revealed that AJs were mainly rearranged into apical zonula adherens between the interface of two epithelial cells in mature lens epithelial cells at 36 hpf (Fig. 1G, S1D, and S1E). In addition, we observed a few junction plaques at basal and lateral interface between epithelia-epithelia were formed at this stage (Fig. 1H and S1E). In posterior lens where epithelial cells were transformed into mesenchymal cells, the apical zonula adherens were disassembled and rearranged as lateral punctum adherens (Fig. 1I and S1F). These observations indicate that a dynamic transition of AJs assembly modes is required for lens development, as frequently observed in development of other organs (Neito et al., 2016).

AJs components fail to accumulate at the apical domains of epithelial cells in *nok* mutants

We then examined the expression patterns of Crb and MPP5 in developing zebrafish lens. Among the isoforms of Crb and MPP5 in zebrafish (Omori and Malicki, 2006; Zou et al., 2010), only the isoforms Crb2a and Nok (Nagie oko, MPP5a homologue in zebrafish), were significantly expressed in zebrafish lens epithelial cells (Fig. 2A-2C and S2A-S2J). Coupling with the apical aggregation of E-cadherin, Crb2a and Nok were not expressed until epidermal-to-epithelial transition occurred (Fig. 2A, 2B, S2A, and S2B). Similar within neuroepithelia, we observed that the apical localization of Crb2a and Nok was reciprocally dependent in lens epithelial cells (Fig. S2C and S2D). Thus we further examined the AJs assembly in *nok* mutant zebrafish.

The point mutation or truncation of Nok with residual domains, such as nok^{m227} and nok^{m520} alleles, remains partial functions (Zou et al., 2013). To obtain clearer results, we generated a *nok* knockout fish line (named as $nok^{ZJUKO203}$ in this study) by CRISPR/Cas9 technique (Fig. S3A-S3D). The Nok protein in this line was truncated at amino acid 38, which is ahead of all conserved domains. A cataract-like phenotype developed in the *nok* mutant zebrafish (Fig. S3E and S3F). Immunostaining of β-catenin, which representing the distribution of AJs, revealed that dysfunction of Nok induced a loss of polarized AJs distribution in lens epithelial cells of *nok* mutants at 36 hpf (Fig. 2C and 2D). TEM revealed that AJs components failed to accumulate at apical domains to form zonula adherens (Fig. 2E). Statistical analysis indicated that AJs were substantially assembled into short punctum adherens and mainly distributed into the basal and lateral interfaces between epithelial and epithelial cells and into the apical interfaces between epithelial and fiber cells, in sharp contradiction to those in WT lens (Fig. 2F). The increase in number of apical AJs between epithelial and fiber cells in *nok* mutants may be partially caused by invasion of epithelial cells into inner lens. The average length of zonula adherens in WT lens epithelial cells was significantly longer than that of punctum adherens (Fig. 2G), implying a more stable lens epithelial structure stabilized by zonula adherens. Whereas, the average length of all types of AJs in *nok* mutants was equivalent to that of punctum adherens, but

significantly shorter than that of zonula adherens (Fig. 2G), suggesting that the stability of epithelial cells may be affected. Indeed, we observed that epithelial cells directly invaded into the inner lens in *nok* mutants (Fig. S4A-S4E, Movie 1-4), resulting in its accumulation in inner lens which cannot be stained by lens fiber cell marker Zl1 (Fig. 2H, 2I, and S4C-S4E; Imai et al., 2010). In contrast, epithelial cells were unable to migrate into inner lens at this stage in WT lens (Fig. S4A; Greiling et al., 2009). The loss of Nok did not affect the differentiation of lens fiber cells, as shown by the Zl1 and Aqp0 staining in lens fiber cells (Fig. 2H, 2I, and S5). At 36 hpf, the number of lens epithelial cells is lower in *nok* mutants than in wild type, whereas the number of lens fiber cells is higher in *nok* mutants than in wild type (Fig. S4F-S4H). The ingressed epithelial cells may progressively differentiate into lens fiber cells in *nok* mutants. Alternatively, the ingressed epithelial cells may be eliminated by cell death and the denucleation of lens fiber cells may be delayed in *nok* mutant. As a result of this abnormal epithelial cells migration, *nok* mutant zebrafish developed a cataract-like phenotype. These data suggest that Nok is required for the proper assembly of AJs that is important in cellular migration.

The apical localization of Nok and Rab11 is reciprocally dependent

Given Rab11 is critical for guiding the vesicle trafficking of AJs, we speculated a possibility for Crb complex-driven regulation of apically oriented trafficking of AJs molecules by Rab11-mediated exocytosis during epidermal-to-epithelial transition in developing lens. We thus first examined the localization of Rab11 in lens. Intriguingly, Rab11 did not exhibit an apical enrichment in epidermal cells at 24 hpf (Fig. 3A), but strongly aggregated at the apical domains in mature epithelial cells where Crb2a was expressed at 36 hpf (Fig. 3B). In contrast, Rab11 lost its apical localization in *nok* mutants at 36 hpf (Fig. 3C). Consistently, both eGFP tagged Rab11a proteins (eGFP-Rab11a) and its constitutive active mutation eGFP-Rab11a Q70L (Chen et al., 1998) enriched well in apical regions in lens epithelial cells in WT zebrafish (Fig. 3D and 3E). However, in *nok* mutants, we observed that eGFP-Rab11 and eGFP-Rab11 Q70L were spread into the apical, lateral and basal regions at comparable eGFP

intensity (Fig. 3F and 3G). The data suggest that the apical distribution of Rab11 requires accurate localization of Crb complex.

To further elucidate this observation, we generated *rab11a*^{ZJUKO233} and *rab11ba*^{ZJUKO234} knockout fish lines by CRISPR/Cas9 technique, considering that Rab11a and Rab11ba are main isoforms in zebrafish lens (Fig. S6; Thisse and Thisse, 2004). We observed that apical distribution of Crb2a required the activity of Rab11, as Crb2a partially lost its apical localization in lens epithelial cells in individual *rab11a* or *rab11ba* knockout mutants (Fig. 3H and 3I). Double knockout (dKO) mutants of *rab11a/rab11ba* completely lost this Crb2a and Nok apical enrichment (Fig. 3J and 3K), suggesting the redundant function of Rab11a with Rab11ba in lens epithelial cells. Consistently, we observed that over-expression of Rab11a S25N, a dominant-negative Rab11 mutant (Chen et al., 1998), but not Rab11a, dose-dependently impeded the apical localization of Nok in lens epithelial cells in WT (Fig. 3L-3O). In detail, either sporadic over-expression generated by plasmid injection (Fig. 3D) or overall over-expression generated by mRNA injection (Fig. 3L) of Rab11a did not significantly affect the apical enrichment of Nok in WT lens epithelial cells. In contrast, lower level over-expression of Rab11a S25N induced the lateral and basal distribution of Nok (Fig. 3N), and higher level of Rab11 S25N significantly impeded the apical aggregation of Nok (Fig. 3M and 3O). Furthermore, different from Rab11a, eGFP tagged Rab11a S25N proteins were spread to the apical, lateral and basal at comparable eGFP intensity in WT lens epithelial cells (Fig. 3N). These observations elucidate that the apical localization of Nok and Rab11 is reciprocally dependent.

The reciprocal dependency between Rab11 and Crb complex was also observed in retinal neuroepithelial cells. Genetic ablation of one Rab11 isoform in retinal neuroepithelial cells weakened the apical distribution of Crb2a, while knockout of two Rab11 isoforms exaggerated this phenotype (Fig. S7A and S7B). In agreement of this observation, Rab11a S25N mutant failed to enrich in the apical regions in WT retinal neuroepithelia, and eGFP-Rab11a also lost the apical enrichment in *nok* mutants (Fig. S7C-S7H).

Rab11 plays critical roles in both exocytosis and endocytosis, and Rab5 plays key roles in endocytosis (Stenmark, 2009; Scott et al., 2014; Woichansky et al., 2016). We thus examined whether the endocytosis pathway was involved in the polarity establishment in lens epithelial cells by over-expressing Rab5 S36N, a dominant negative form of Rab5 (Stenmark et al., 1994), in zebrafish embryos. Different from the over-expression of Rab11a S25N, we observed that the sporadic over-expression of Rab5 S36N did not affect the apical localization of Nok in WT lens epithelial cells (Fig. 3P), suggesting endocytosis is not involved in the Nok localization in lens epithelial cells. Interestingly, we indeed observed Nok proteins was ectopically present in fiber cells in WT lens over-expressing either Rab5 S36N or Rab11a S25N (Fig. 3K-3P), suggesting an important role of endocytosis on breaking down the apical polarity in lens mesenchymal/fiber cells during epithelial-to-mesenchymal and fiber cells transition. These data suggest that Crb complex may guide apically oriented vesicle exocytosis mediated by Rab11 in epithelial cells with different origin.

MPP5 physically associates with rab11 to promote their reciprocal apical localization

Given reciprocal dependency between Rab11 and Crb complex, we speculated that component(s) of Crb complex may directly interact with Rab11 to guide the orientated exocytosis of AJs molecules. We thus inspected the interaction between Rab11 and a variety of polarity proteins by co-immunoprecipitation assays. As expected, Nok but not other polarity proteins examined strongly interacted with Rab11a (Fig. 4A), albeit that Par complex and Par5 were reported to be involved in Rab11-mediated vesicle exocytosis (Bryant et al., 2010; Winter et al., 2012). Domain mapping analysis revealed that L27-PDZ-SH3 domain (a.a. 151-505) of Nok was necessary and sufficient for Rab11a interaction (Fig. 4B). Surprisingly, Rab11a S25N, the dominant negative mutant of Rab11, was unable to interact with Nok, while the constitutive active Rab11a (Q70L) exhibited a stronger Nok interaction (Fig. 4C). Importantly, we observed Rab11 form an endogenous complex with Pals1 (MPP5a homologue in mammals), but not the other tested polarity proteins, in MDCK cells, a

widely used in vitro model for studies of polarization (Simmons, 1982; Chavrier et al., 1990) (Fig. 4D). The Co-immunoprecipitation results using zebrafish eye extracts further confirmed that Rab11 interacted with Nok in zebrafish (Fig. 4E). The data suggest a complex formed by Nok and Rab11, which may determine the function of Rab11 in vesicle exocytosis.

We then investigated whether Crb or Par complex affect the cellular distribution of AJs in HEK293T cells. We observed that co-expression of Crb2a and Nok induced a significant increase of membrane association of β-catenin comparing with the neighbor control cells which were transfection negative (Fig. 4G and 4K). In contrast, the expression of eGFP did not affect the expression and localization of β-catenin (Fig. 4F and 4K), and the expression of aPKCλ and Pard6 promoted the level of β-catenin in cytoplasmic, but not significantly induced its membrane associated distribution (Fig. 4H and 4K). As expected, expression of Rab11a S25N, but not Rab11a, substantially impeded the phenotype driven by co-expression of Crb2a and Nok (Fig. 4I-4K). Furthermore, we observed that eGFP-Rab11a, Nok-mCherry and eGFP-Rab11a S25N were spread in the whole cell without aggregation when these proteins were individually expressed in MDCK cells (Fig. S8A-S8C). However, eGFP-Rab11a, and Nok-mCherry were aggregated into dot-like foci when these two proteins were co-expressed (Fig. 4L-4P). As the control, the co-expression of eGFP-Rab11a S25N and Nok-mCherry did not display the similar phenotype (Fig. S8D). We observed that about 29% of eGFP-Rab11a foci and 41% of Nok-mCherry foci were co-localized in Golgi but not endoplasmic reticulum (Fig. 4N). These data suggest that the Nok-Rab11 complex is formed mainly in Golgi. These data suggest that Nok, rather than other polarity proteins, forms a previously unrecognized complex with Rab11, to orientate the exocytosis of AJs components.

Rab11 determines the localization and assembly of AJs

We then investigated whether Rab11 dysfunction phenocopies the AJs remolding defects, similar as the dysfunction of Crb complex. We observed a compromised β-catenin aggregation at the apical domains in lens epithelial cells of *rab11a*^{ZJUKO233} or *rab11ba*^{ZJUKO234} mutants, which was further exaggerated when both were ablated (Fig. 5A-5H). Alike with dysfunction of Crb complex, double ablation of *rab11a* and *rab11ba* prevented the formation of zonula adherens (Fig. 5I and 5K-5M). Interestingly, the number of apical punctum adherens between lens epithelial and fiber cells significantly reduced in *rab11a/rab11ba* dKO mutants (Fig. 5K), suggesting an important roles of Rab11 in the formation of AJs_EF. Single *rab11a* or *rab11ba* knockout partially affected the number and average length of AJs_EE, but did not induce a significant change of AJs_EF (Fig. 5K and 5L), likely because of the redundant function of these two proteins. More AJs molecules appeared to be transported into the lateral regions to form punctum adherens (Fig. 5K and 5M). Consistent with these observations, Rab11a S25N disrupted the apical enrichment of β-catenin (Fig. 5E and 5F) and the proper AJs remodeling during epidermal-to-epithelial transition, a phenotype similar as *rab11a/rab11ba* dKO or the dysfunction of Nok (Fig. 5J-5M). The data suggest that Rab11-mediated transporting of AJs molecules is entering into apical regions both between epithelia-epithelia and between epithelia-fiber cells, but not just to the limited apical domains between epithelial cells as previously known.

The apical localization of aPKC is not associated with Rab11

Par complex is also known to be involved in apical zonula adherens formation in epithelial cells (Joberty et al., 2000). Intriguingly, our data indicated that key components of the Par complex, including aPKCλ, Pard6, and Pard3, failed to interact with Rab11 (Fig. 4A), implying a distinct mechanism of Par complex participating in AJs remodeling. Immunostaining of aPKC showed a much earlier and more extensive expression pattern than the components of Crb complex (Fig. 6A-6C). In particular, aPKC was expressed but only enriched at the apical domains when Crb2a was

expressed and epidermal-to-epithelial transition started (Fig. 6A and 6B). Diverse with the restrictive expression of Crb2a in epithelia, aPKC was also expressed in mesenchymal and primary fiber cells and displayed a non-polarized distribution (Fig. 6C). We observed that aPKCλ ablation resulted in the disappearance of apical zonula adherens in mature lens epithelial cells (Fig. 6D). Intriguingly, phenotypes of *aPKCλ* mutants in AJs remodeling appeared to be associated with the expression of Crb complex, as in lens epidermal cells or in surface epidermis cells where Crb complex is absent, ablation of aPKCλ exhibited no significant phenotype (Fig. 6E).

To elucidate whether the apical localization of aPKC and Rab11 is reciprocally dependent, we examined the localization of Crb2a, Rab11, aPKC and F-actin in *aPKCλ*, *rab11a/rab11ba* and *nok* mutants. In $aPKC\lambda^{m567}$ mutants, the immunostaining signal of aPKC was lost, and actin also lost its apical enrichment (Fig. 6F). Interestingly, we frequently observed a heterogeneity for the localization of Crb2a and Rab11 in lens epithelial cells in *aPKCλ* mutants. Specifically, both Crb2a and Rab11 lost their apical localization in most of lens epithelial cells (63%, n=167 cells in 10 retinas) in *aPKCλ* mutants. However, Rab11a was co-localized with Crb2a in the lens epithelial cells in which Crb2a was localized at the apical domains (Fig. 6G). In *rab11a/rab11ba* dKO mutants, immunohistochemistry results clearly showed that Rab11, Crb2a and Nok were all lost in lens epithelial cells (Fig. 3J, 3K, 6H and 6I). However, both aPKC and actin were nicely enriched at the apical regions (Fig. 6H and 6I). In *nok* mutants, we also frequently observed a heterogeneity for the apical localization of aPKC between anterior and lateral lens epithelial cells. The immunostaining signals showed that both Crb2a and Rab11 concurrently lost their apical enrichment in lateral lens epithelial cells in *nok* mutants (Fig. 3C). However, aPKC and F-actin still displayed apical enrichment in lateral lens epithelial cells in *nok* mutants (Fig. 6J and 6K). The mechanism through which the heterogeneity is induced remains largely unknown yet, probably some proteins (such as Pak1) may play redundant functions (Aguilar-Aragon et al., 2018). Together with the observations on the localization of Crb2a, Rab11, aPKC, and F-actin in WT and mutants, and the fact that Nok interacts with Rab11, we conclude that the apical

localization of aPKC is not associated with Rab11, which is different from Crb-MPP5a complex.

Cytoskeletal modulation is also involved in the vesicle trafficking (Lanzetti, 2007; Horgan and McCaffrey 2011). The dynamic assembly of Par complex is known to regulate the actin and microtubule cytoskeleton organization (Uberall et al., 1999; Betschinger et al., 2003; Harris and Peifer, 2007), and aPKC modulates the orientation of actomyosin cables to facilitate Rab11-mediated exocytosis in the *Drosophila* airway tubes (Hosono et al., 2015). Consistent with these reports, we observed that the apical enrichment of F-actin is closely associated with aPKC localization in lens epithelia, rather than localization of Crb complex (Fig. 6F-6H and 6J). Taking together, these data imply that aPKC may affect the AJs remodeling through cytoskeleton modulation.

DISCUSSION

The cell state and the type of AJs can be accurately identified, which makes the developing vertebrate lens an ideal model to investigate the cell state transition and AJs remodeling *in vivo*. Using this model, here we proposed a molecular model where Crb and Par complexes were synergized to promote the Rab11-mediated remodeling of AJs. Crb and Par complexes are known to play conserved roles in modulating cell behaviors in many organs derived from epithelia crossing *Drosophila* to mammals (Tepass, 2012; Chen and Zhang, 2013; Campanale et al., 2017). Our data indicate that the apical localization of Crb complex is dose-dependently associated with Rab11. Loss of single *rab11* isoform partially disrupts the apical localization of Crb complex and AJs remodeling in epithelia, while loss of more *rab11* isoforms leads to a severer phenotype. The association between Rab11 and the Crb complex occurs in both mature lens epithelial cells and retinal neuroepithelial cells. The slight presence of apical enrichment of Crb2a in retinal neuroepithelial cells (Fig. S7A and S7B) might be caused by the redundant functions of other *rab11* isoforms, such as *rab11bb* (Thisse and Thisse, 2004). The model proposed in this study for coordination of AJs

remodeling and cell migration pattern may apply to other epithelia-derived tissues as well.

Because of the functional association, ablation of Rab11, the Crb complex or the Par complex leads to the similar defects in AJs modeling in epithelial cells. However, we illustrated here that distinct complexes play each specific role in organizing AJs remodeling. The Crb complex orientates the AJs_EE vesicle traffic of AJs molecules and stabilizes them into zonula adherens through the direct MPP5a-Rab11 interplay. One possibility is that the dysfunction of Crb complex leads to the stochastic orientation of Rab11-mediated vesicle traffic to apical interface between epithelial and fiber cells (AJs_EF) and lateral interface between epithelia-epithelia (LJs_EE).

Distinct from the epithelial specific expression of Crb complex, Par complex is also expressed in epidermal cells, mesenchymal cells and tumor cells (Fig. 6; Halaoui and McCaffrey, 2015). The expression of Par complex in mesenchymal cells and tumor cells cannot induce the formation of apical zonula adherens, which also suggests the disappearance of zonula adherens caused by aPKC dysfunction is mediated indirectly through Crb complex. Thus, we speculated that, by stabilizing the apical membrane localization of Crb complex and by modulating cytoskeleton to facilitate the Rab11-mediated vesicle exocytosis, Par complex promotes the formation of apical polarity and zonula adherens in epithelial cells. When the Crb complex and adherens components are transported to the apical domains in epithelia, aPKC may separate AJs from Crb complex via phosphorylating the Crb and Par3, thus defining the apical/lateral border (Sotillos et al., 2004; Morais-de-Sa et al., 2010; Wei et al., 2015).

Both endocytosis and exocytosis pathways play important roles in the remodeling of AJs (Stenmark, 2009; Scott et al., 2014; Woichansky et al., 2016). In this study, we observed that the dysfunction of Rab5, a key regulator of early endosome (Chavrier et al., 1990; Gorvel et al., 1991; Barbieri et al., 1996), did not affect the apical localization of Nok, suggesting that the endocytosis pathway is not involved in the polarity formation in lens epithelial cells. During the epidermal-to-epithelial transition of lens cells, we observed that most of AJs were converted from tricellular adherens

and punctum adherens in lens epidermal cells to AJs_EE (zonula adherens) and AJs_EF (punctum adherens) in lens epithelial cells (Fig. 2F). In *rab11a/rab11ba* dKO mutants, both the AJs_EE and the AJs_EF in lens epithelial cells significantly decreased (Fig. 5K), suggesting an important roles of Rab11 in the formation of these apical AJs. Given that Rab11 play roles in both endocytosis and exocytosis pathways (Ullrich et al., 1996; Chen et al., 1998; Woichansky et al., 2016), the precise role of endocytosis and exocytosis in the formation of AJs_EE and AJs_EF remains to be elucidated in future study.

In sum, our data identified a novel MPP5a-Rab11 complex. The interplay between Nok and Rab11 synergistically establish the apical polarity as well as the formation of zonula adherens during the maturation of epithelial cells, probably through the regulation of the apical exocytosis.

Materials and Methods

Zebrafish strains

Zebrafish were bred and maintained in accordance with Zhejiang University Animal Care and Use Committee protocols. AB WT, *crb2a*^{m289} (Oromi and Malicki, 2006), *aPKCλ*^{m567} (Horne-Badovinac et al., 2001), *nok*^{ZJUKO203} (this study), *rab11a*^{ZJUKO233} (this study), and *rab11a*^{ZJUKO234} (this study) were used in this study. Embryos were collected and kept in E3 embryo buffer (5 mM NaCl, 0.17 mM KCl, 0.33 mM $CaCl_2$ and 0.33 mM $MgSO_4$). Embryos were grown at 28 °C in an incubator.

Generation of knockout zebrafish using CRISPR-Cas9

SgRNAs (final concentration at 25-50 pg per embryo) targeting to *nok*, *rab11a* and *rab11ba* genes and mRNA of Cas9 (final concentration at 50-100 pg per embryo) were co-injected into AB WT embryos at 1-cell stage. Founder fish were raised to adulthood and outcrossed with AB WT fish to obtain F1 generation. The generated knockout lines were nominated as *nok*^{ZJUKO203}, *rab11a*^{ZJUKO233} and *rab11a*^{ZJUKO234} respectively in this study. Heterozygous F1 adult zebrafish outcrossed with AB WT

fish to obtain F2 generation. Heterozygous F2 fish incrossed to obtain homozygous mutant embryos for the analyses.

In vitro transcription of RNA and micro-injection

RNAs were transcripted *in vitro* using the mMESSAGE mMACHINE kit (Thermo Fisher Scientific, AM1344). For mRNA injection, we injected 50-100 pg mRNA into AB WT embryos at 1-cell stage. For plasmid injection, as much as 25 pg of plasmid along with 50 pg of Tol2 transposase *mRNA* was co-injected into zebrafish embryos. To examine the effects of over-expression of Rab11 or Rab5, we generated plasmids pTol2-*EF1*::eGFP-Rab11a, pTol2-*EF1*::eGFP-Rab11a S25N, pTol2-*EF1*:: eGFP-Rab11a Q70L, and pTol2-*EF1*::eGFP-Rab5 S36N (Clark et al., 2011). For the sporadic over-expression of N-terminal eGFP tagged Rab proteins shown in Fig. 3D-3G and 3N-3P, we injected the plasmids pTol2-*EF1*::eGFP-Rab11a, pTol2-*EF1*:: eGFP-Rab11a S25N, pTol2-*EF1*::eGFP-Rab11a Q70L, or pTol2-*EF1*::eGFP-Rab5 S36N together with Tol2 transposase mRNA to zebrafish embryos. For the mRNA over-expression shown in Fig. 3L, 3M, 5E and 5F, we generated plasmids pCS2-eGFP-2A-Rab11a and pCS2-eGFP-2A-Rab11a S25N, adding 2A peptide between eGFP and Rab11a by overlapping PCR based on the above constructs. Peptide 2A could self-cleave the proteins eGFP-2A-Rab11 and eGFP-2A-Rab11-S25N to release free eGFP (as the expression marker) and target proteins to avoid the mutual interference between eGFP and the target proteins. We injected eGFP-2A-Rab11a and eGFP-2A-Rab11a S25N mRNA into zebrafish embryos.

Time-lapse imaging

The plasmid *pTol2-H2A::eGFP* was injected into WT and *nok*^{ZJUKO203} embryos at 1-cell stage to mosaically label lens cells. At 28 hpf, the embryos expressing eGFP in lens were mounted in 1% low-melting-point agarose in E3 embryo medium with 168 mg/l tricaine for anaesthetization in a glass-bottom FluoroDish (World Precision Instrument). Embryos were imaged using 10X-dipping objectives on a Nikon A1

confocal microscope. The lens epithelial cells labeled with eGFP were imaged every 10 or 30 minutes since 28 hpf. The time-lapse imaging lasted 2 hours from 28 hpf to 30 hpf.

Immunohistochemistry and antibodies

The following antibodies were used: anti-Aqp0 (1:200, Millipore AB3071), anti-Zl1 (1:200, Abcam ab185979), anti-β-catenin (1:200, Sigma C7207), anti-E-cadherin (1:100, BD transduction 610182, Arora et al., 2020), anti-ZO1 (1:200, Invitrogen 339100), anti-Nok (1:200, generated in-house, Zou et al., 2008), anti-Pals1 (1:2000 for immunoblotting, Millipore 07-708), anti-Ponli (1:200, generated in-house, Zou et al., 2010), anti-Crb1 (1:200, generated in-house, Zou et al., 2012), anti-Crb2a (1:200, generated in-house in rabbit, Zou et al., 2012), anti-Crb2b (1:200, generated in-house, Zou et al., 2012), anti-Crb2a (1:200, mouse monoclonal antibody, ZIRC zs-4), anti-aPKC (1:200, Santa Cruz, sc216), anti-Rab11 (1:100, CST2413s. The polyclonal antibodies recognize the residues surrounding Arg184 of human Rab11a protein.). Alexa Fluor 488 Phalloidin (1:300, Life tech A12379) and Alexa Fluor 647 Phalloidin (1:100, Life tech A22287) were used to visualize F-actin. Dapi (Thermo Fisher Scientific, D3571) was used to stain nuclei. Immunohistochemistry were performed using the procedure described previously (Zou et al., 2008). Confocal microscopy was performed using a Nikon A1 confocal microscope. Adobe Photoshop 7.0 was used for subsequent image processing. For all immunohistochemistry experiments, we repeated each experiment at least three times, and at least 10 embryos were analyzed for each experiment.

Transmission electron microscopy

The embryos at desired developmental stage were fixed in 2% electron microscope (EM) grade glutaraldehyde plus 2% paraformaldehyde in 0.1M PBS (pH 7.3) at 4 ^{o}C, rinsed in PBS, postfixed with 1% OsO_4 and 0.1% $K_3Fe(CN)_6$, dehydrated through a graded series of ethanol, and embedded in Epon (Energy Beam Sciences, East Granby, CT, USA). 65-nm ultrathin tissue sections were stained with 2% uranyl acetate and

Reynold's lead citrate and then examined with a Hitachi Model H-7650 transmission EM.

Cell culture, transfections and immunofluorescence

HEK293T and MDCK cells were obtained from ATCC and cultured in DMEM medium with 10% fetal bovine serum (FBS) at 37 °C in 5% CO_2 (v/v). For the immunofluorescence experiments, HEK293T cells were transfected with the plasmids specified in the results section for 24 hours (plasmids expressing eGFP, Crb2a and Nok, Crb2a and Nok and mCherry-Rab11a, Crb2a and Nok and mCherry-Rab11a S25N, aPKCλ-eGFP and Pard6γb respectively), using Xtremegene HP (Roche) or polythylenimine (PEI, Polysciences) transfection reagents. The transfected cells were fixed in 4% paraformaldehyde, permeablized, blocked in 2% BSA and 0.1% Triton X-100 in PBS for 30 min, and incubated sequentially with primary antibodies anti-Crb2a or anti-β-catenin and Alexa-labeled secondary antibodies with extensive washing. Immunofluorescence images were obtained using the Nikon A1 confocal microscope.

Co-immunoprecipitations and immunoblottings

HEK293T cells transfected for 24 hours with specific plasmids encoding amino-terminal Myc-, HA- and Flag- tagged Rab11a, Crb2a$^{\Delta EX}$, Nok, Par5ζ, Par5θ, aPKCλ, Par6γb, and Pard3, were lysed by modified Myc lysis buffer (MLB) (20 mM Tris-Cl, 200 mM NaCl, 10 mM NaF, 1 mM NaV_2O_4, 1% NP-40, 20 mM β-glycerophosphate, and protease inhibitor, pH 7.5). Cell lysates were then subjected to immunoprecipitation using anti-Flag or anti-HA antibodies for transfected proteins, or using anti-Rab11/PALS1 antibodies for endogenous proteins of MDCK cells. After 2-3 washes with MLB, adsorbed proteins in beads were resolved by 1X SDS loading buffer and analyzed by SDS-PAGE and immunoblotting with indicated antibodies. Cell lysates were also analyzed by SDS-PAGE and immunoblotting to control protein abundance.

Quantifications

Adobe Photoshop 7.0 (Adobe) was used to quantify the length of adhesion plaques imaged by TEM, and was used to quantify the fluorescence intensity imaged by confocal microscope. Prism 6.0b (Graphpad) was used to plot graphs and for statistical analyses. The value of adhesion plaques per epithelium shown in Fig. 2F and 5K was defined by the sum of the number of adhesion plaques divided by the number of epithelial cells for each lens. We compared the membrane associated β-catenin intensity in the transfection positive cells (Fig. 4F-4J, marked by *) with that in the transfection negative neighbor cells (Fig. 4F-4J, marked by #). The value of relative intensity of membrane associated β-catenin was shown in Fig. 4K was defined by the intensity in the cells in Fig. 4F-4J marked with * divided by that in the cells marked by #. The co-expressed eGFP-rab11a and Nok-mCherry proteins were spread broadly in MDCK cells with aggregation in Golgi. The images were read with Adobe Photoshop 7.0 (Adobe) and the value of percentage of triple positive foci shown in Fig. 4N and defined by the Rab11/Nok/GM130 triple positive foci divided by the total Rab11 positive foci or Nok positive foci. The value of apical / basal relative intensity shown in Fig. 5H, 6I and 6K was defined by the fluorescence intensity of apical spot at the vertex point between two epithelial cells (green spot in schematic illustration Fig. 5G) divided by the fluorescence intensity of basal spot (red spot, same size with the green spot). In each lens, 5 anterior epithelial cells and 8 lateral epithelial cells (4 dorsal and 4 ventral cells) were measured. 20 lenses from 10 embryos were imaged and used for the quantification analyses. The value of fiber cells / epithelial cells ratio shown in Fig. S4H was defined by the nuclei number of inner lens cells divided by the nuclei number of epithelial cells in the same lens.

Statistics

Five embryos for TEM related quantitative analyses and at least 10 embryos for immunohistochemistry related quantitative analyses of each experiment were used in this study. Immunohistochemistry, time-lapse imaging and cell culture related experiments were repeated a minimum of three independent times to ensure reproducibility. Data are expressed as mean ± SEM. Differences were analyzed by two-tailed Student's t test using Prism 6 (GraphPad Software, La Jolla, USA), p values < 0.05 were considered significant. No statistical method was used to predetermine sample size. The investigators were not blinded to allocation during experiments and outcome assessment.

ACKNOWLEDGEMENTS

We are grateful to J. Peng and X. Feng (Zhejiang University) for valuable suggestions. The work was supported by Natural Science Foundation of Zhejiang Province (project LZ15H120001 to J.Z.), National Natural Science Foundation of China (projects 81770938 to J.Z., 81800807 to X.T., and 81570822 to K.Y.), and the Fundamental Research Funds for the Central Universities (2016FZA7010 and 2017FZA7001 to J.Z., and 2017FZA7002 to X.T.).

AUTHOR CONTRIBUTIONS

Y.H., Y.Z. and Y.Y carried out most experiments, M.Z., Q.Z., K.W., and J.L. contributed to several experiments. X.T., P.X., B.L., and K.Y. helped with data analyses and discussions. J.Z. designed experiments, analyzed the data and wrote the paper.

DECLARATION OF INTERESTS

The authors declare no competing interests.

REFERENCES

Aguilar-Aragon, M., Elbediwy, A., Foglizzo, V., Fletcher, G.C., Li, V.S.W., Thompson, B. J. (2018). Pak1 kinase maintains apical membrane identity in epithelia. *Cell Rep.* 7, 1639-1646.

Apodaca, G., Gallo, L.I., and Bryant, D.M. (2012). Role of membrane traffic in the generation of epithelial cell asymmetry. *Nat. Cell Biol.* **14**, 1235-1243.

Arora, P., Dongre, S., Raman, R., and Sonawane, M. (2020). Stepwise polarisation of developing bilayered epidermis is mediated by aPKC and E-cadherin in zebrafish. *Elife* **9**.

Balda, M.S., and Matter, K. (2016). Tight junctions as regulators of tissue remodelling. *Curr. Opin. Cell Biol.* **42**, 94-101.

Barbieri, M.A., Roberts, R.L., Mukhopadhyay, A., and Stahl, P.D. (1996). Rab5 regulates the dynamics of early endosome fusion. *Biocell* **20**, 331-338.

Betschinger, J., Mechtler, K., and Knoblich, J.A. (2003). The Par complex directs asymmetric cell division by phosphorylating the cytoskeletal protein Lgl. *Nature* **422**, 326-330.

Bruser, L., and Bogdan, S. (2017). Adherens Junctions on the Move-Membrane Trafficking of E-Cadherin. *Cold Spring Harb. Perspect. Biol.* **9 (3)**.

Bryant, D.M., Datta, A., Rodriguez-Fraticelli, A.E., Peranen, J., Martin-Belmonte, F., and Mostov, K.E. (2010). A molecular network for de novo generation of the apical surface and lumen. *Nat. Cell Biol.* **12**, 1035-1045.

Bulgakova, N.A., and Knust, E. (2009). The Crumbs complex: from epithelial-cell polarity to retinal degeneration. *J. Cell Sci.* **122**, 2587-2596.

Campanale, J.P., Sun, T.Y., and Montell, D.J. (2017). Development and dynamics of cell polarity at a glance. *J. Cell Sci.* **130**, 1201-1207.

Chavrier, P., Parton, R.G., Hauri, H.P., Simons, K., and Zerial, M. (1990). Localization of low molecular weight GTP binding proteins to exocytic and endocytic compartments. *Cell* **62**, 317-329.

Chen, J., and Zhang, M. (2013). The Par3/Par6/aPKC complex and epithelial cell polarity. *Exp. Cell Res.* **319**, 1357-1364.

Chen, W., Feng, Y., Chen, D., and Wandinger-Ness, A. (1998). Rab11 is required for trans-golgi network-to-plasma membrane transport and a preferential target for GDP dissociation inhibitor. *Mol. Biol. Cell* **9**, 3241-3257.

Clark, B.S., Winter, M., Cohen, A.R., and Link, B.A. (2011). Generation of Rab-based transgenic lines for in vivo studies of endosome biology in zebrafish. *Dev. Dyn.* **240**, 2452-2465.

Fletcher, G.C., Lucas, E.P., Brain, R., Tournier, A., and Thompson, B.J. (2012). Positive feedback and mutual antagonism combine to polarize Crumbs in the Drosophila follicle cell epithelium. *Curr. Biol.* **22**, 1116-1122.

Flores-Benitez, D., and Knust, E. (2015). Crumbs is an essential regulator of cytoskeletal dynamics and cell-cell adhesion during dorsal closure in Drosophila. *Elife* **4**.

Gorvel, J.P., Chavrier, P., Zerial, M., and Gruenberg, J. (1991). rab5 controls early endosome fusion in vitro. *Cell* **64**, 915-925.

Greiling, T.M., and Clark, J.I. (2009). Early lens development in the zebrafish: a three-dimensional time-lapse analysis. *Dev. Dyn.* **238**, 2254-2265.

Halaoui, R., and McCaffrey, L. (2015). Rewiring cell polarity signaling in cancer. *Oncogene* **34**, 939-950.

Harris, K.P., and Tepass, U. (2008). Cdc42 and Par proteins stabilize dynamic adherens junctions in the Drosophila neuroectoderm through regulation of apical endocytosis. *J. Cell Biol.* **183**, 1129-1143.

Harris, T.J., and Peifer, M. (2007). aPKC controls microtubule organization to balance adherens junction symmetry and planar polarity during development. *Dev. Cell* **12**, 727-738.

Harris, T.J., and Tepass, U. (2010). Adherens junctions: from molecules to morphogenesis. *Nat. Rev. Mol. Cell Biol.* **11**, 502-514.

Horgan, C.P., and McCaffrey, M.W. (2011). Rab GTPases and microtubule motors. *Biochem. Soc. Trans.* **39**, 1202-1206.

Horne-Badovinac, S., Lin, D., Waldron, S., Schwarz, M., Mbamalu, G., Pawson, T., Jan, Y., Stainier, D.Y., and Abdelilah-Seyfried, S. (2001). Positional cloning of

heart and soul reveals multiple roles for PKC lambda in zebrafish organogenesis. *Curr. Biol.* **11**, 1492-1502.

Hosono, C., Matsuda, R., Adryan, B., and Samakovlis, C. (2015). Transient junction anisotropies orient annular cell polarization in the Drosophila airway tubes. *Nat. Cell Biol.* **17**, 1569-1576.

Hsu, Y.C., Willoughby, J.J., Christensen, A.K., and Jensen, A.M. (2006). Mosaic Eyes is a novel component of the Crumbs complex and negatively regulates photoreceptor apical size. *Development* **133**, 4849-4859.

Hurd, T.W., Gao, L., Roh, M.H., Macara, I.G., and Margolis, B. (2003). Direct interaction of two polarity complexes implicated in epithelial tight junction assembly. *Nat. Cell Biol.* **5**, 137-142.

Imai, F., Yoshizawa, A., Fujimori-Tonou, N., Kawakami, K., and Masai, I. (2010). The ubiquitin proteasome system is required for cell proliferation of the lens epithelium and for differentiation of lens fiber cells in zebrafish. *Development* **137**, 3257-3268.

Joberty, G., Petersen, C., Gao, L., and Macara, I.G. (2000). The cell-polarity protein Par6 links Par3 and atypical protein kinase C to Cdc42. *Nat. Cell Biol.* **2**, 531-539.

Klebes, A., and Knust, E. (2000). A conserved motif in Crumbs is required for E-cadherin localisation and zonula adherens formation in Drosophila. *Curr. Biol.* **10**, 76-85.

Korol, A., Pino, G., Dwivedi, D., Robertson, J.V., Deschamps, P.A., and West-Mays, J.A. (2014). Matrix metalloproteinase-9-null mice are resistant to TGF-beta-induced anterior subcapsular cataract formation. *Am. J. Pathol.* **184**, 2001-2012.

Lanzetti, L. (2007). Actin in membrane trafficking. *Curr. Opin. Cell Biol.* **19**, 453-458.

Laprise, P., Beronja, S., Silva-Gagliardi, N.F., Pellikka, M., Jensen, A.M., McGlade, C.J., and Tepass, U. (2006). The FERM protein Yurt is a negative regulatory component of the Crumbs complex that controls epithelial polarity and

apical membrane size. *Dev. Cell* **11**, 363-374.

Morais-de-Sa, E., Mirouse, V., and St Johnston, D. (2010). aPKC phosphorylation of Bazooka defines the apical/lateral border in Drosophila epithelial cells. *Cell* **141**, 509-523.

Nieto, M.A., Huang, R.Y., Jackson, R.A., and Thiery, J.P. (2016). Emt: 2016. *Cell* **166**, 21-45.

Omori, Y., and Malicki, J. (2006). oko meduzy and related crumbs genes are determinants of apical cell features in the vertebrate embryo. *Curr. Biol.* **16**, 945-957.

Park, B., Alves, C.H., Lundvig, D.M., Tanimoto, N., Beck, S.C., Huber, G., Richard, F., Klooster, J., Andlauer, T.F., Swindell, E.C., et al. (2011). PALS1 is essential for retinal pigment epithelium structure and neural retina stratification. *J. Neurosci.* **31**, 17230-17241.

Penkert, R.R., DiVittorio, H.M., and Prehoda, K.E. (2004). Internal recognition through PDZ domain plasticity in the Par-6-Pals1 complex. *Nat. Struct. Mol. Biol.* **11**, 1122-1127.

Ramkumar, N., Omelchenko, T., Silva-Gagliardi, N.F., McGlade, C.J., Wijnholds, J., and Anderson, K.V. (2016). Crumbs2 promotes cell ingression during the epithelial-to-mesenchymal transition at gastrulation. *Nat. Cell Biol.* **18**, 1281-1291.

Roeth, J.F., Sawyer, J.K., Wilner, D.A., and Peifer, M. (2009). Rab11 helps maintain apical crumbs and adherens junctions in the Drosophila embryonic ectoderm. *PLoS One* **4**, e7634.

Scott, C.C., Vacca, F., and Gruenberg, J. (2014). Endosome maturation, transport and functions. *Semin. Cell Dev. Biol.* **31**, 2-10.

Simmons, N.L. (1982). Cultured monolayers of MDCK cells: a novel model system for the study of epithelial development and function. *Gen. Pharmacol.* **13**, 287-291.

Sobajima, T., Yoshimura, S., Iwano, T., Kunii, M., Watanabe, M., Atik, N., Mushiake, S., Morii, E., Koyama, Y., Miyoshi, E., et al. (2014). Rab11a is required for apical protein localisation in the intestine. *Biol. Open* **4**, 86-94.

Sotillos, S., Diaz-Meco, M.T., Caminero, E., Moscat, J., and Campuzano, S. (2004). DaPKC-dependent phosphorylation of Crumbs is required for epithelial cell

polarity in Drosophila. *J. Cell Biol.* **166**, 549-557.

Stenmark, H. (2009). Rab GTPases as coordinators of vesicle traffic. *Nat. Rev. Mol. Cell Biol.* **10**, 513-525.

Stenmark, H., Parton, R.G., Steele-Mortimer, O., Lutcke, A., Gruenberg, J., and Zerial, M. (1994). Inhibition of rab5 GTPase activity stimulates membrane fusion in endocytosis. *EMBO J.* **13**, 1287-1296.

Thisse B., Thisse C. (2004). Fast Release Clones: A High Throughput Expression Analysis. http://zfin.org/ZDB-PUB-040907-1.

Tepass, U. (1996). Crumbs, a component of the apical membrane, is required for zonula adherens formation in primary epithelia of Drosophila. *Dev. Biol.* **177**, 217-225.

Tepass, U. (2012). The apical polarity protein network in Drosophila epithelial cells: regulation of polarity, junctions, morphogenesis, cell growth, and survival. *Annu. Rev. Cell Dev. Biol.* **28**, 655-685.

Uberall, F., Hellbert, K., Kampfer, S., Maly, K., Villunger, A., Spitaler, M., Mwanjewe, J., Baier-Bitterlich, G., Baier, G., and Grunicke, H.H. (1999). Evidence that atypical protein kinase C-lambda and atypical protein kinase C-zeta participate in Ras-mediated reorganization of the F-actin cytoskeleton. *J. Cell Biol.* **144**, 413-425.

Ullrich, O., Reinsch, S., Urbe, S., Zerial, M., and Parton, R.G. (1996). Rab11 regulates recycling through the pericentriolar recycling endosome. *J. Cell Biol.* **135**, 913-924.

van de Pavert, S.A., Meuleman, J., Malysheva, A., Aartsen, W.M., Versteeg, I., Tonagel, F., Kamphuis, W., McCabe, C.J., Seeliger, M.W., and Wijnholds, J. (2007). A single amino acid substitution (Cys249Trp) in Crb1 causes retinal degeneration and deregulates expression of pituitary tumor transforming gene Pttg1. *J. Neurosci.* **27**, 564-573.

Wei, Z., Li, Y., Ye, F., and Zhang, M. (2015). Structural basis for the phosphorylation-regulated interaction between the cytoplasmic tail of cell polarity protein crumbs and the actin-binding protein moesin. *J. Biol. Chem.* **290**,

11384-11392.

Winter, J.F., Hopfner, S., Korn, K., Farnung, B.O., Bradshaw, C.R., Marsico, G., Volkmer, M., Habermann, B., and Zerial, M. (2012). Caenorhabditis elegans screen reveals role of PAR-5 in RAB-11-recycling endosome positioning and apicobasal cell polarity. *Nat. Cell Biol.* **14**, 666-676.

Woichansky, I., Beretta, C.A., Berns, N., and Riechmann, V. (2016). Three mechanisms control E-cadherin localization to the zonula adherens. *Nat. Commun.* **7**, 10834.

Yonemura, S. (2011). Cadherin-actin interactions at adherens junctions. *Curr. Opin. Cell Biol.* **23**, 515-522.

Zou, J., Lathrop, K.L., Sun, M., and Wei, X. (2008). Intact retinal pigment epithelium maintained by Nok is essential for retinal epithelial polarity and cellular patterning in zebrafish. *J. Neurosci.* **28**, 13684-13695.

Zou, J., Wang, X., and Wei, X. (2012). Crb apical polarity proteins maintain zebrafish retinal cone mosaics via intercellular binding of their extracellular domains. *Dev. Cell* **22**, 1261-1274.

Zou, J., Wen, Y., Yang, X., and Wei, X. (2013). Spatial-temporal expressions of Crumbs and Nagie oko and their interdependence in zebrafish central nervous system during early development. *Int. J. Dev. Neurosci.* **31**, 770-782.

Zou, J., Yang, X., and Wei, X. (2010). Restricted localization of ponli, a novel zebrafish MAGUK-family protein, to the inner segment interface areas between green, red, and blue cones. *Invest. Ophthalmol. Vis. Sci.* **51**, 1738-1746.

Figures

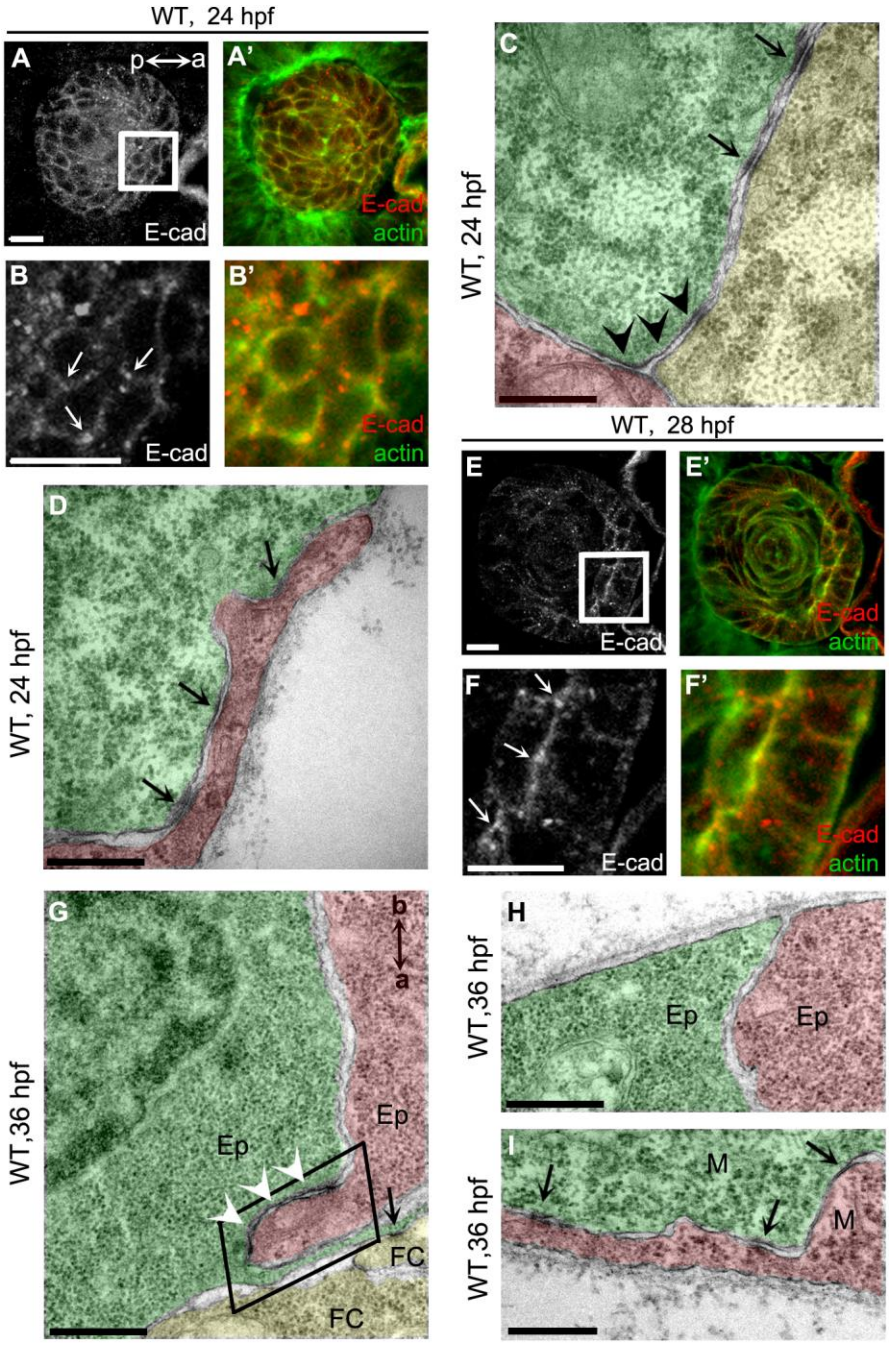

Figure 1. AJs are dynamically remodeled during lens cell state transition.

(A-D) E-cadherin was non-polarly distributed in lens epidermal cells at 24 hpf. Arrows show the punctuated accumulation of E-cadherin at the vertex points where three neighbor epidermal cells meet (B). B is the higher magnifications of the white boxed regions in A. a (anterior) and p (posterior) in panel A show the lens orientation. (C and D) Tricellular adherens (C, black arrowheads) and lateral punctum adherens

(D, arrows) were the major adhesion plaques between lens epidermal cells in WT at 24 hpf. Punctum adherens existed at the lateral (C) and basal (D) regions.

(E and F) E-cadherin was enriched in the apical regions of epithelial cells when epidermal-to-epithelial transition occurred at 28 hpf (E and F). Arrows show the punctuated accumulation of E-cadherin in the apical regions of epithelial cells (F). F is the higher magnifications of the white boxed regions in E.

(G-I) AJs were assembled into zonula adherens at the apical domain between epithelia-epithelia (white arrowheads) (G). Few adhesion plaques were observed in the basal regions between epithelia-epithelia in WT at 36 hpf (H). Lateral punctum adherens, but not apical zonula adherens were observed between mesenchymal cells when epithelial-to-mesenchymal transition occurred (I). The black boxed region in G shows the apical zone between two epithelial cells. Ep, epithelium; M, mesenchymal cells; FC, fiber cells. a (apical) and b (basal) in panel G show the orientation of lens epithelial cells. The lower magnification TEM images to show the position of 1C, 1D, and 1G-1I in lens was presented in Fig. S1.

Scale bar, 10 μm (A, B, E, and F) and 400 nm (C, D, and G-I).

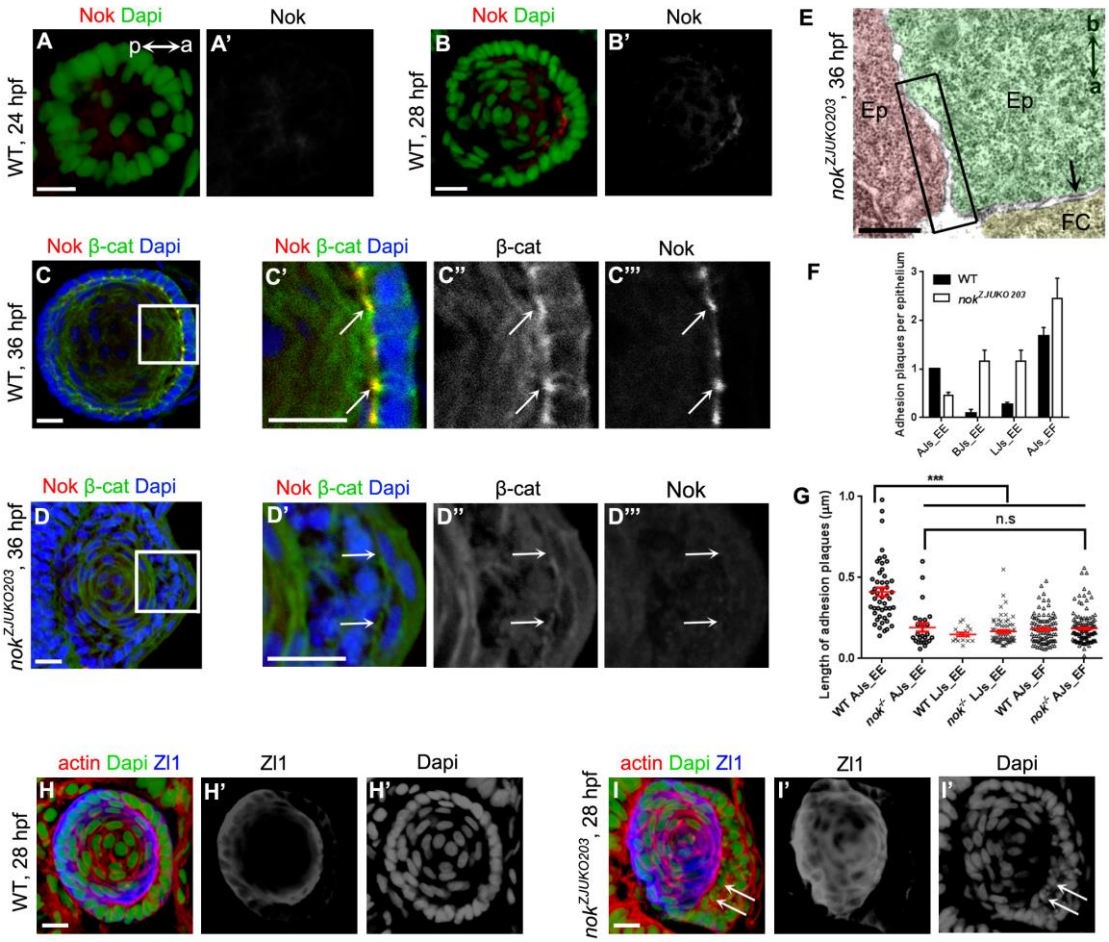

Figure 2. AJs components fail to accumulate at the apical domains of epithelial cells in *nok* mutants

(A) Nok was not expressed in lens epidermal cells at 24 hpf. a (anterior) and p (posterior) in panel A show the lens orientation.

(B) Nok started to be expressed in lens epithelial cells at 28 hpf when epidermal-to-epithelial transition occurred.

(C and D) Apical enriched β-catenin co-localized with Nok in WT lens epithelial cells at 36 hpf. β-catenin lost its apical enrichment in *nok* mutants at 36 hpf. C'-C''' and D'-D''' are higher magnifications of the white boxed regions in C and D respectively.

(E) Apical zonula adherens disappeared in *nok* mutants at 36 hpf. a (apical) and b (basal) show the orientation of lens epithelial cells.

(F) Quantification of the number of adhesion plaques in lens epithelial cells in WT and *nok* at 36 hpf. In WT lens, the apical AJs between epithelia-epithelia (AJs_EE, 1

per epithelia) and the apical AJs between epithelia-fiber cells (AJs_EF, 1.68 per epithelia) constituted the major types of adhesion plaques. In *nok* mutants, AJs_EE number significantly decreased (0.45 per epithelia), and number of other types of adhesion plaques, including the basal AJs between epithelia-epithelia (BJs-EE), the lateral AJs between epithelia-epithelia (LJs-EE) and AJs-EF, significantly increased.

(G) Quantification of the length of adhesion plaques in epithelial cells in WT and *nok* mutants at 36 hpf. The length of AJs_EE (e=0.41 μm ± 0.03) was significantly longer than LJs_EE (e=0. 15 μm ± 0.01) and AJs_EF (e=0.18 μm ± 0.01) in WT. The length of AJs_EE in *nok* mutants (e=0.19 μm ± 0.02) was significantly reduced and comparable with LJs_EE and AJs_EF. n = 49 epithelial cells for WT and 59 for *nok* mutants.

(H and I) Compared with WT (H), a large number of Zl1-immunoreactivity negative cells (arrows) accumulated in inner lens in *nok* mutants at 28 hpf (I).

Scale bar, 10 μm (A-D, H and I) and 400 nm (E). ***P<0.001, n.s>0.05.

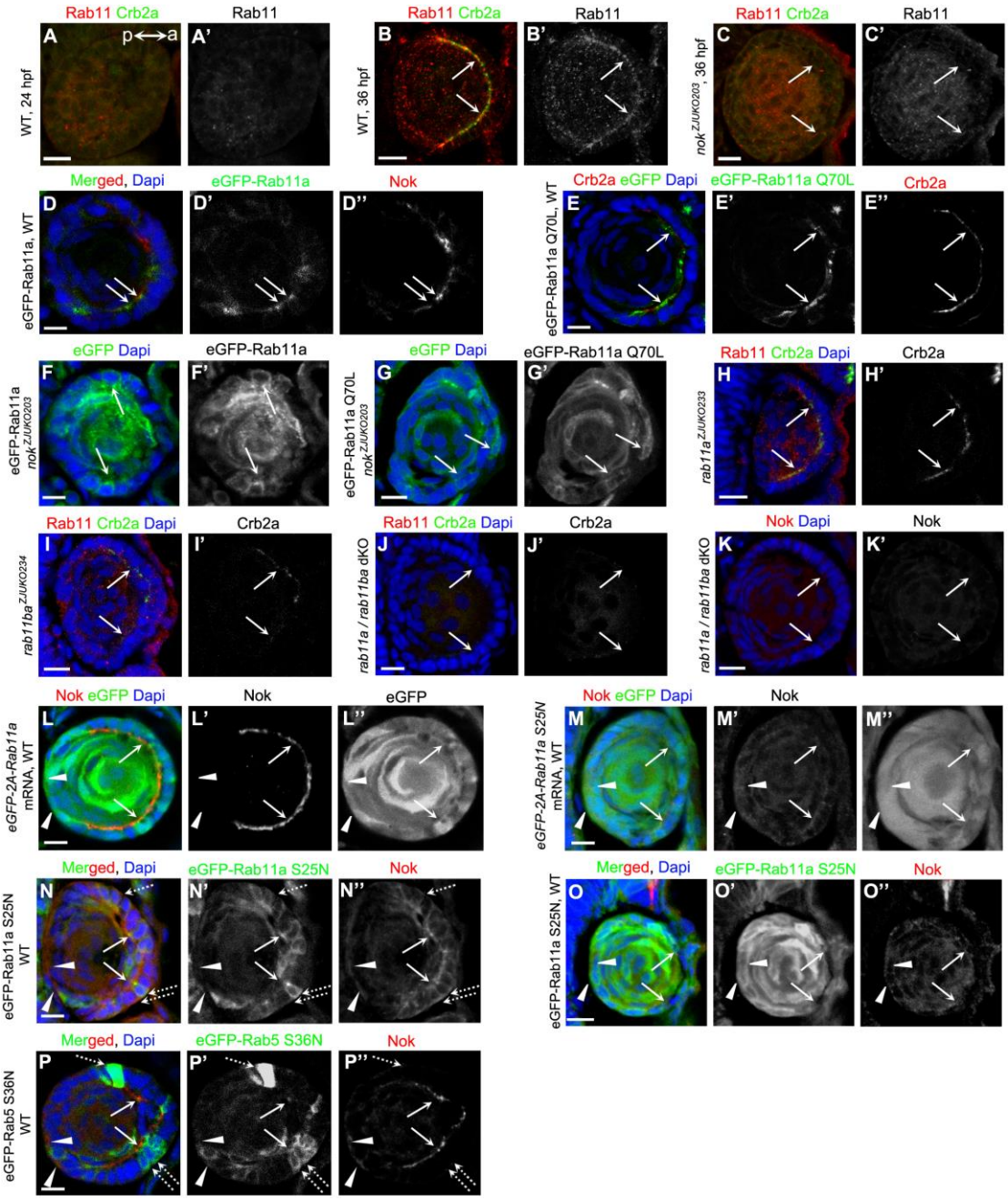

Figure 3. The apical localization of Nok and Rab11 is reciprocally dependent

(A and B) Temporospatial expression pattern of Rab11 in zebrafish lens. Rab11 did not display polarized aggregation in epidermal cells when Crb2a was not detectable at 24 hpf (A), but strongly aggregated in the apical regions in lens epithelial cells at 36 hpf (B). a (anterior) and p (posterior) in panel A show the lens orientation.

(C) Rab11 lost its apical enrichment in lens epithelial cells in *nok* mutants.

(D-E) eGFP tagged Rab11a (D) and Rab11 Q70L (E) proteins were enriched in the

apical regions in lens epithelial cells in WT. Over-expression of eGFP-Rab11a and Rab11 Q70L did not significantly affect the apical enrichment of Nok.

(F-G) eGFP tagged Rab11a (F) and Rab11 Q70L (G) proteins were distributed at the lateral and basal regions in lens epithelial cells in *nok* mutants.

(H-K) The apical localization of Crb2a in lens epithelial cells was disrupted partially in *rab11a* (H) or *rab11ba* mutants (I), and completely in *rab11a/rab11ba* dKO mutants (J). Similar with Crb2a, the apical localization of Nok was lost in *rab11a/rab11ba* dKO mutants (K).

(L and M) Over-expression of eGFP-2A-Rab11a (L) or eGFP-2A-Rab11a S25N (M) by mRNA injections. Over-expression of Rab11a S25N (M), but not Rab11a (L) impeded the apical aggregation of Nok. Low level of Nok was observed in mesenchymal cells over-expressed with eGFP-2A-Rab11a S25N in posterior lens (M, white triangles).

(N-O) eGFP-Rab11a S25N is evenly spread to apical, lateral and basal regions in WT lens epithelial cells. Lower level over-expression of eGFP-Rab11a S25N induced the lateral and basal distribution of Nok (N), and higher level of eGFP-Rab11a S25N impeded the apical aggregation of Nok (O). Low level of Nok was observed in mesenchymal cells over-expressed with eGFP-Rab11a S25N in posterior lens (N and O, white triangles).

(P) Over-expression of eGFP-Rab5 S36N did not significantly affect the apical enrichment of Nok in WT lens epithelial cells. Low level of Nok (white triangles) was observed in mesenchymal cells over-expressed with eGFP-Rab5 S36N in posterior lens.

The embryos used for B-P were fixed at 36 hpf. Arrows show the apical regions of lens epithelial cells. Broken arrows show the basal regions of lens epithelial cells. White triangles show the fiber cells in posterior lens. Plasmids pTol2-*EF1*::eGFP-Rab11a, pTol2-*EF1*::eGFP-Rab11a S25N, pTol2-*EF1*:: eGFP-Rab11a Q70L, or pTol2-*EF1*:: eGFP-Rab5 S36N was used for the sporadic over-expression of eGFP tagged Rab proteins shown in Figures 3D-3G and 3N-3P.

Scale bar, 10 μm.

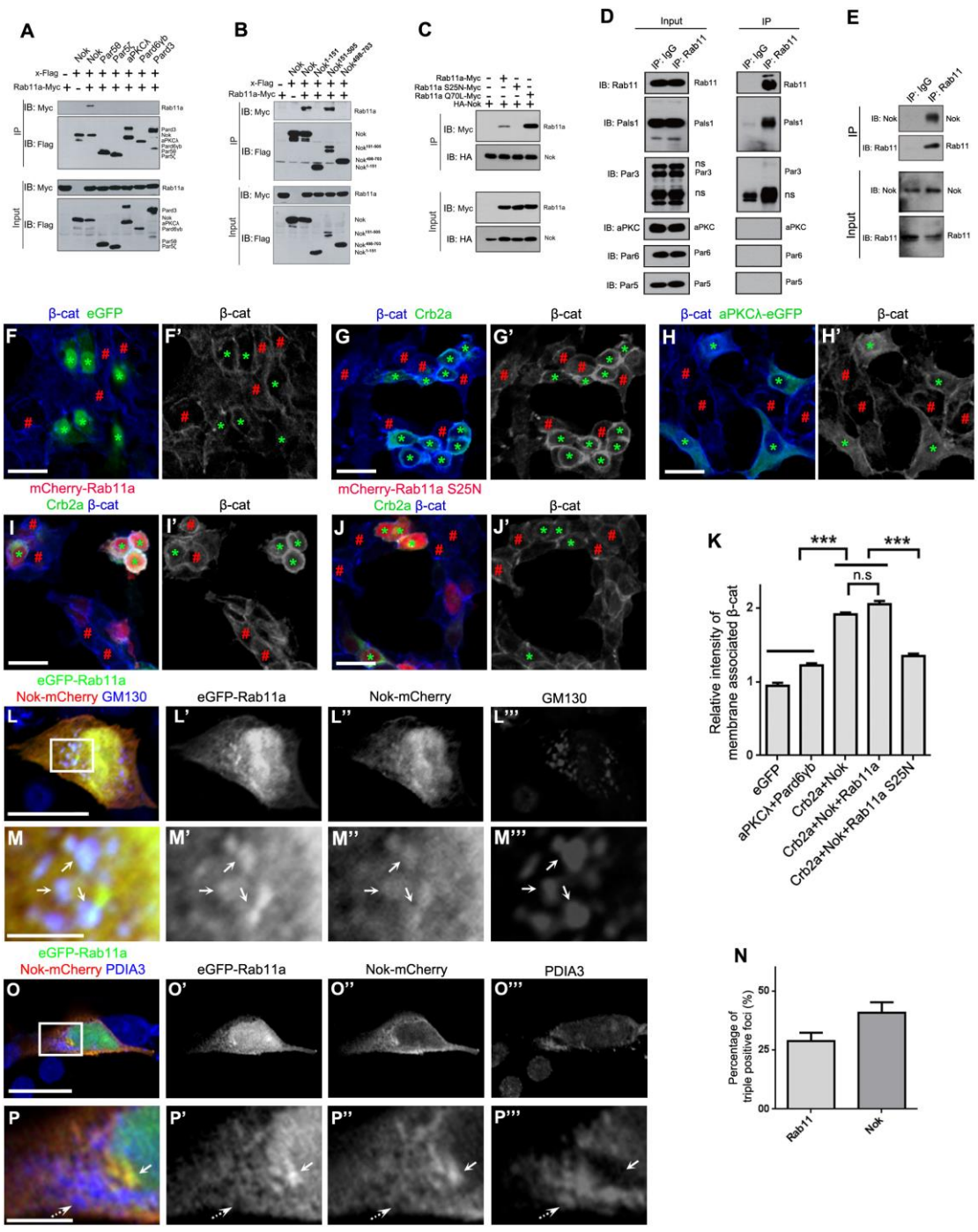

Figure 4. Nok interplays with Rab11 to promote membrane association of β-catenin in human cultured cells

(A) Nok, but not other polarity proteins examined, including Par5θ, Par5ζ, aPKCλ, Pard6γb and Pard3, interacted with Rab11a.

(B) The L27-SH3-PDZ domain of Nok ($Nok^{151-505}$) interacted with Rab11a.

(C) The dominant negative Rab11a (S25N) did not interact with Nok, while the

constitutively active Rab11a (Q70L) had a higher affinity with Nok than wild-type Rab11a.

(D) Co-immunoprecipitation verified the endogenous complex between Rab11 and Nok, but not the other tested proteins, in MDCK cells.

(E) Co-immunoprecipitation using zebrafish eye extracts verified the endogenous complex between Nok and Rab11 in zebrafish.

(F-H) Co-expression of Crb2a and Nok (G), but not co-expression of aPKCλ and Pard6γb (H), or the expression of eGFP (F) promoted the membrane association of β–catenin in HEK293T cells.

(I and J) The expression of Rab11a S25N (J), but not Rab11a (I) impeded the membrane association of β–catenin induced by co-expression of Crb2a and Nok in HEK293T cells.

(K) Quantification of fluorescence intensity of membrane associated β–catenin shown in F-J. n > 60 cells.

(L-P) eGFP-Rab11a was co-localized with Nok-mCherry in Golgi (L and M, labeled by GM130), but not in endoplasmic reticulum (O and P, labeled by PDIA3) in MDCK cells. M and P are higher magnifications of the white boxed regions in L and O, respectively. Arrows show the aggregation of eGFP-Rab11a and Nok-mCherry, broken arrow shows endoplasmic reticulum. N is the quantification of the percentage of triple positive foci in rab11a-positive foci and Nok-positive foci shown in L. n > 60 cells.

Scale bar, 20 μm (F-J), 10 μm (L and O), and 2.5μm (M and P). ***P<0.001, n.s>0.05.

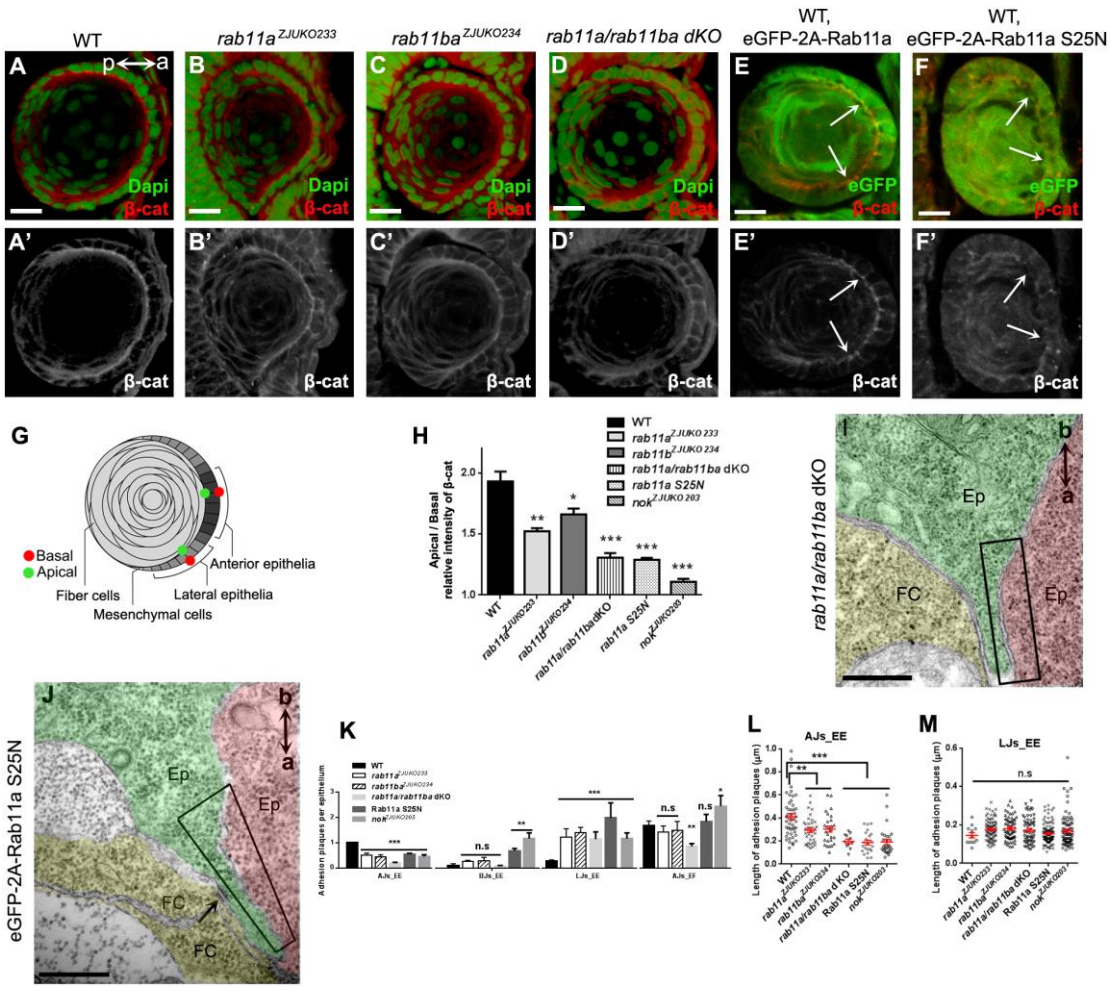

Figure 5. Rab11 determines the localization and assembly of AJs

(A-F) The distribution of β–catenin in WT (A), *rab11a* (B), *rab11ba* (C), *rab11a/rab11ba* dKO (D), eGFP-2A-Rab11a over-expressed (E) and eGFP-2A-Rab11a S25N over-expressed (F) embryos at 36 hpf. a (anterior) and p (posterior) in panel A show the lens orientation. Arrows in E and F show eGFP-2A-Rab11a S25N, but not eGFP-2A-Rab11a, impeded the apical enrichment of β-catenin.

(G and H) Quantification of apical/basal relative intensity of β–catenin showed in A-F. G is the schematic illustration of H. n = 20 lenses from 10 embryos.

(I and J) Both dKO of *rab11a/rab11ba* (I) and over-expression of Rab11a S25N (J) disrupted the AJs_EE zonula adherens at 36 hpf. Arrow shows AJs_EF punctum adherens. a (apical) and b (basal) show the orientation of lens epithelial cells.

(K) Over-expression of Rab11a S25N or *rab11a/rab11ba* dKO significantly impeded

the formation of AJs_EE. The number of AJs_EF also significantly decreased in *rab11a/rab11ba* dKO mutants. n = 56 epithelial cells for *rab11a/rab11ba* dKO mutants, and 73 for Rab11a S25N over-expressed embryos.

(L) The length of AJs_EE in Rab11a S25N over-expressed or *rab11a/rab11ba* dKO mutant lens (e=0.19 µm ± 0.02) was comparable with that in *nok* mutants, and significantly shorter than that in WT.

(M) Although the number of LJs_EE significantly increased in Rab11a S25N over-expressed or *rab11a/rab11ba* dKO mutant lens (e=0.15 µm ± 0.01), the length of LJs_EE was comparable with that in WT and *nok* mutants.

Scale bar, 10 µm (A-F) and 400 nm (I and J). **P<0.01, ***P<0.001, n.s>0.05.

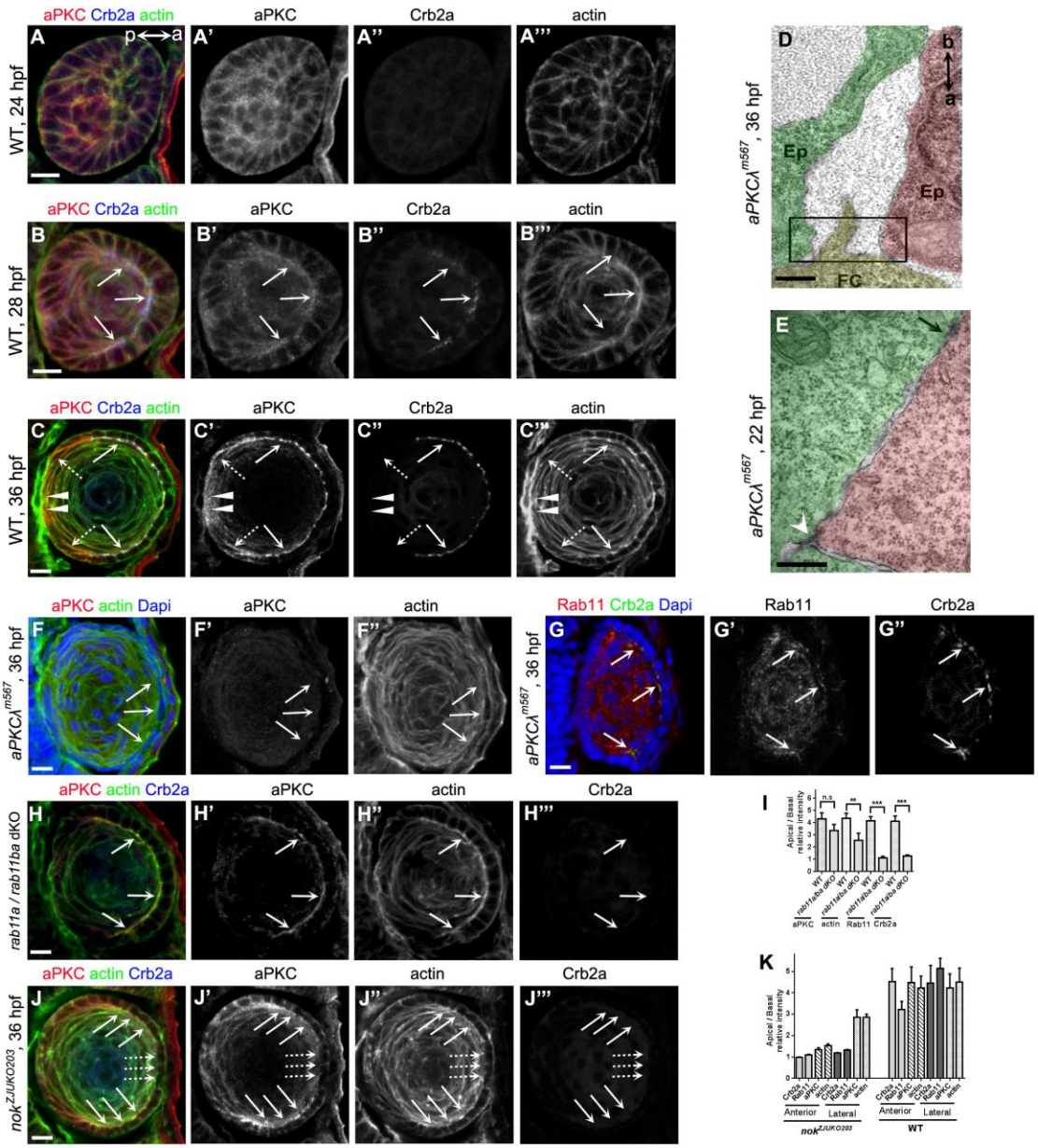

Figure 6. aPKC organizes cytoskeleton to promote AJ remodeling, but apical localization of aPKC does not require Rab11

(A-C) Temporospatial expression pattern of aPKC in zebrafish lens. aPKC displays non-polarized distribution in lens epidermal cells when Crb2a was not expressed at 24 hpf (A). Coupling with Crb2a expression in epithelia, aPKC was accumulated to the apical domains at 28 hpf (B). aPKC was restricted at the apical domains and co-localized with Crb2a in epithelial cells at 36 hpf (C). Different from Crb2a, aPKC was also expressed in lens mesenchymal cells (broken arrows) and primary fiber cells (arrowheads) (C). Arrows in B and C show the apical aggregation of aPKC, Crb2a

and actin in lens epithelial cells. Broken arrows show the lens mesenchymal cells. Arrowheads show the primary fiber cells. a (anterior) and p (posterior) in panel A show the lens orientation.

(D) Apical zonula adherens disappeared in lens epithelial cells in *aPKCλ* mutants at 36 hpf. a (apical) and b (basal) show the orientation of lens epithelial cells. The black boxed region in D shows the apical zone between two epithelial cells.

(E) Tricellular adherens (white arrowhead) and lateral punctum adherens (arrow) existed between lens epidermal cells in *aPKCλ* mutants at 22 hpf.

(F and G) In *aPKCλ* mutants, aPKC staining was disappear (F), actin lost its apical enrichment (F), and Crb2a and Rab11 lost their apical distribution in most of epithelial cells at 36 hpf (G). Arrows in F show the apical regions of lens epithelial cells. Arrows in G show the apical co-localization of Crb2a and Rab11.

(H) In *rab11a*/*rab11ba* dKO mutants, Crb2a lost its apical aggregation at 36 hpf. In contrast, aPKC and actin still enriched at the apical domains in lens epithelial cells. Arrows show the apical regions of lens epithelial cells.

(I) Quantification of apical/basal relative fluorescence intensity of aPKC, actin, Crb2a and Rab11 in WT and *rab11a*/*rab11ba* dKO mutants shown in Fig. 6H. aPKC displayed normal apical enrichment in *rab11a*/*rab11ba* dKO mutant lens epithelial cells; however, apical enrichment of actin, Crb2a and Rab11 is significantly decreased although actin reduction is mild. n = 20 lenses from 10 embryos.

(J) The apical localization of aPKC and actin displayed a heterogeneity in different lens epithelial cells in *nok* mutants at 36 hpf. Broken arrows show aPKC and actin lost their apical enrichment in the anterior epithelial cells. Arrows show aPKC and actin were still enriched in the apical regions in lateral epithelial cells.

(K) Quantification of apical/basal relative fluorescence intensity of aPKC, actin, Crb2a and Rab11 in *nok* mutants shown in Fig. 6J and 3C. The apical enrichment of actin was associated with aPKC, while the apical enrichment of Rab11 was associated with Crb2a. Crb2a and aPKC showed concurrent apical localization only in anterior epithelia, but not in lateral epithelial cells. n = 20 lenses from 10 embryos.

Scale bar, 10 μm (A-C, and F-I) and 400 nm (D and E). **P<0.01, ***P<0.001.

Figure S1

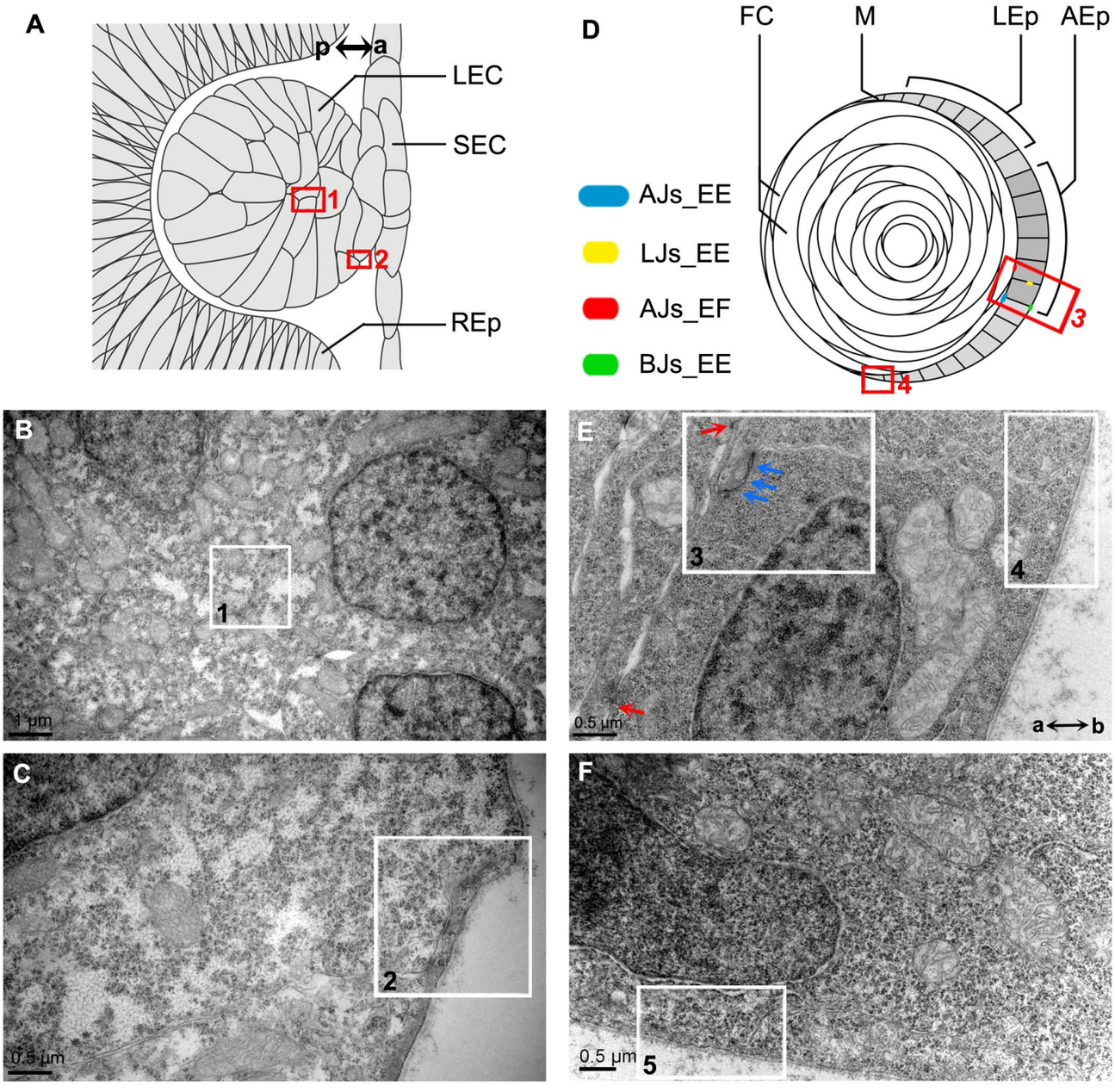

Figure S1. Dynamical remodeling of AJs in lens cells during lens development.

(A) The schematic illustration of zebrafish lens at 24 hpf. Red box 1 shows the position of B in lens. Red box 2 shows the position of C in lens.

(B and C) Representative TEM images of inner lens (B) and surface of lens (C). Higher magnifications of white box 1 and 2 regions are shown in Figure 1C and 1D, respectively.

(D) The schematic illustration of zebrafish lens at 36 hpf. Red box 3 shows the position of E in lens. Red box 4 shows the position of F in lens.

(E and F) Representative TEM images of lens epithelial cells (E) and mesenchymal cells (F). Higher magnifications of white box 3-5 regions are shown in Figure 1G-1I, respectively. a (apical) and b (basal) in panel E show the orientation of lens epithelial cells.

Figure S2

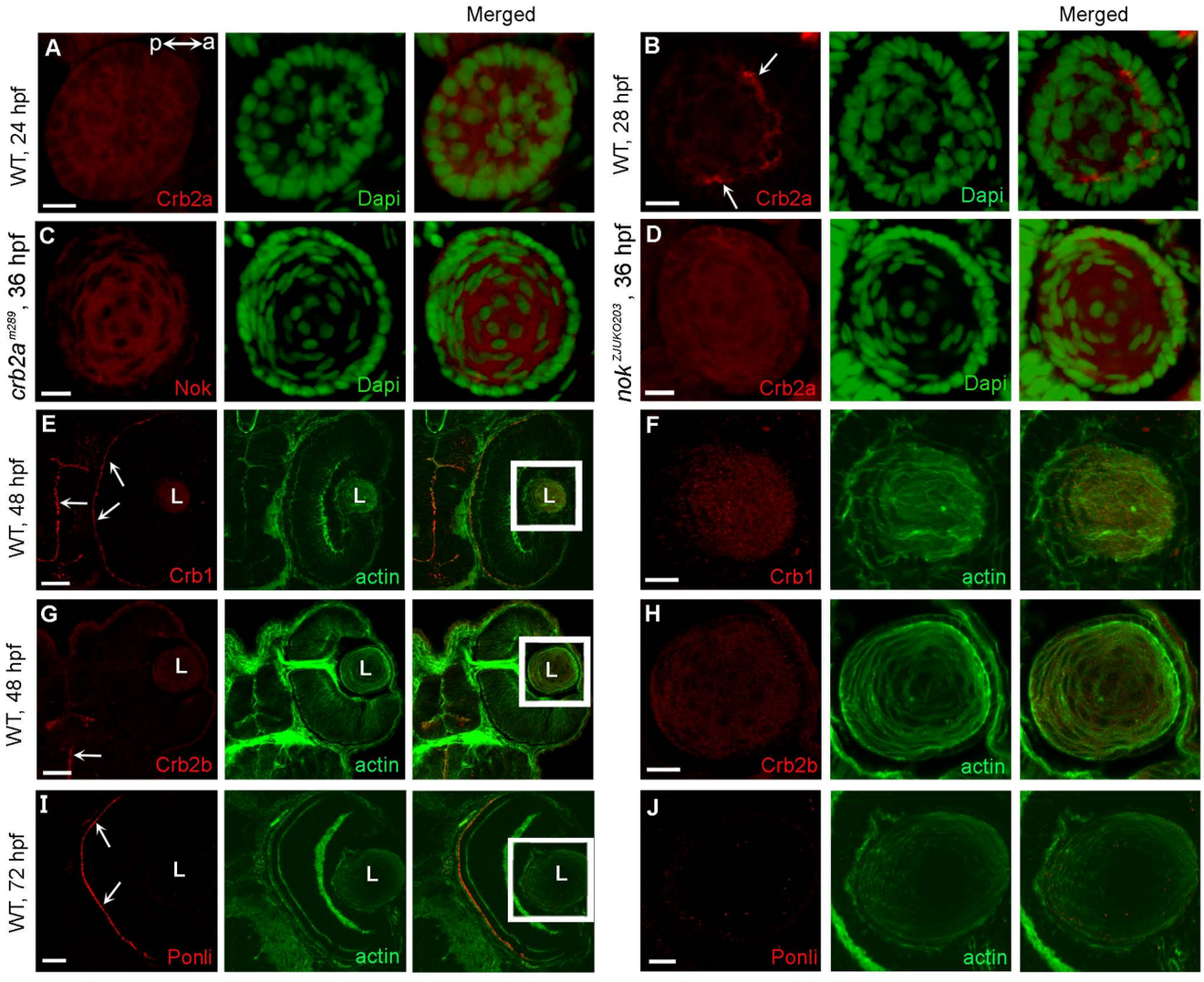

Figure S2. Nok and Crb2a, but not other isoforms, are expressed in lens epithelial cells.

(A and B) Crb2a started to be expressed in lens epithelial cells at 28 hpf (B), but not in lens epidermal cells at 24 hpf (A). Arrows show the apical regions of lens epithelial cells. a (anterior) and p (posterior) in panel A show the lens orientation.

(C and D) The apical localization of Nok (C) and Crb2a (D) was reciprocally dependent in lens epithelial cells at 36 hpf.

(E-J) The other isoforms, including Crb1 (E and F), Crb2b (G and H) and Ponli (MPP5b homologue in zebrafish, I and J) were not expressed in zebrafish lens. F, H and J are the higher magnifications of boxed regions in E, G and I respectively.

Scale bar, 10 μm (A-D, F, H and J), 20 μm (E, G and I). L in panel E, G and I, lens.

Figure S3

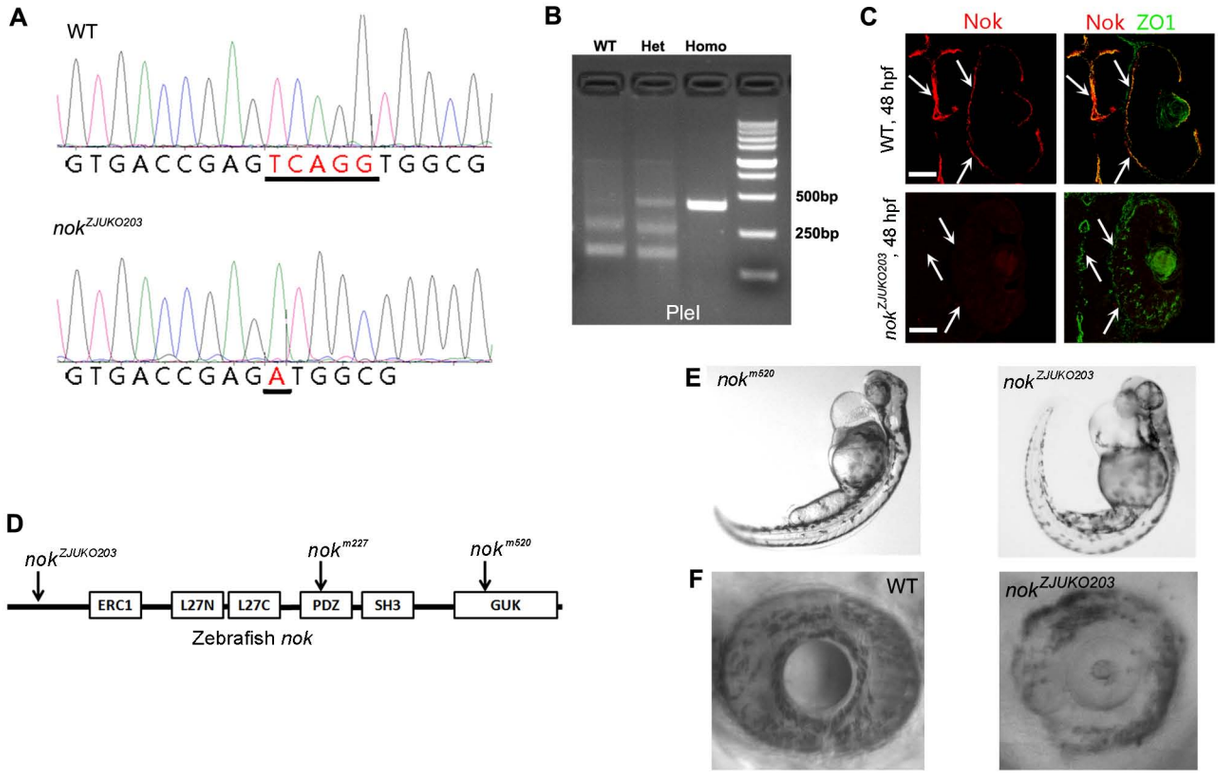

Figure S3. Generation of *nok* mutant zebrafish.

(A) Sanger sequencing results showed that 4 nucleotides were deleted in the *nok*^{ZJUKO203} mutants, causing the loss of restriction enzyme Ple I recognition site.

(B) The *nok*^{ZJUKO203} mutants were genotyped with PCR followed by digestion with PleI. The PCR product of WT (404 bp) could be digested with Ple I into two fragments (160 bp and 244 bp). The PCR product of *nok*^{ZJUKO203} mutants could not be digested with Ple I.

(C) Immunostaining using anti-Nok antibodies showed that the gene was successfully knocked out in *nok*^{ZJUKO203} mutants. Arrows show the apical regions of retina and brain where Nok should enrich.

(D) The schematic illustration of the mutated position of *nok* gene.

(E) The general phenotype caused by *nok*^{ZJUKO203} knockout was similar to *nok*^{m520} allele, 96 hpf.

(F) Cataract-like phenotype was visible in *nok*^{ZJUKO203} mutants at 96 hpf.

Scale bar, 20 μm (C).

Figure S4

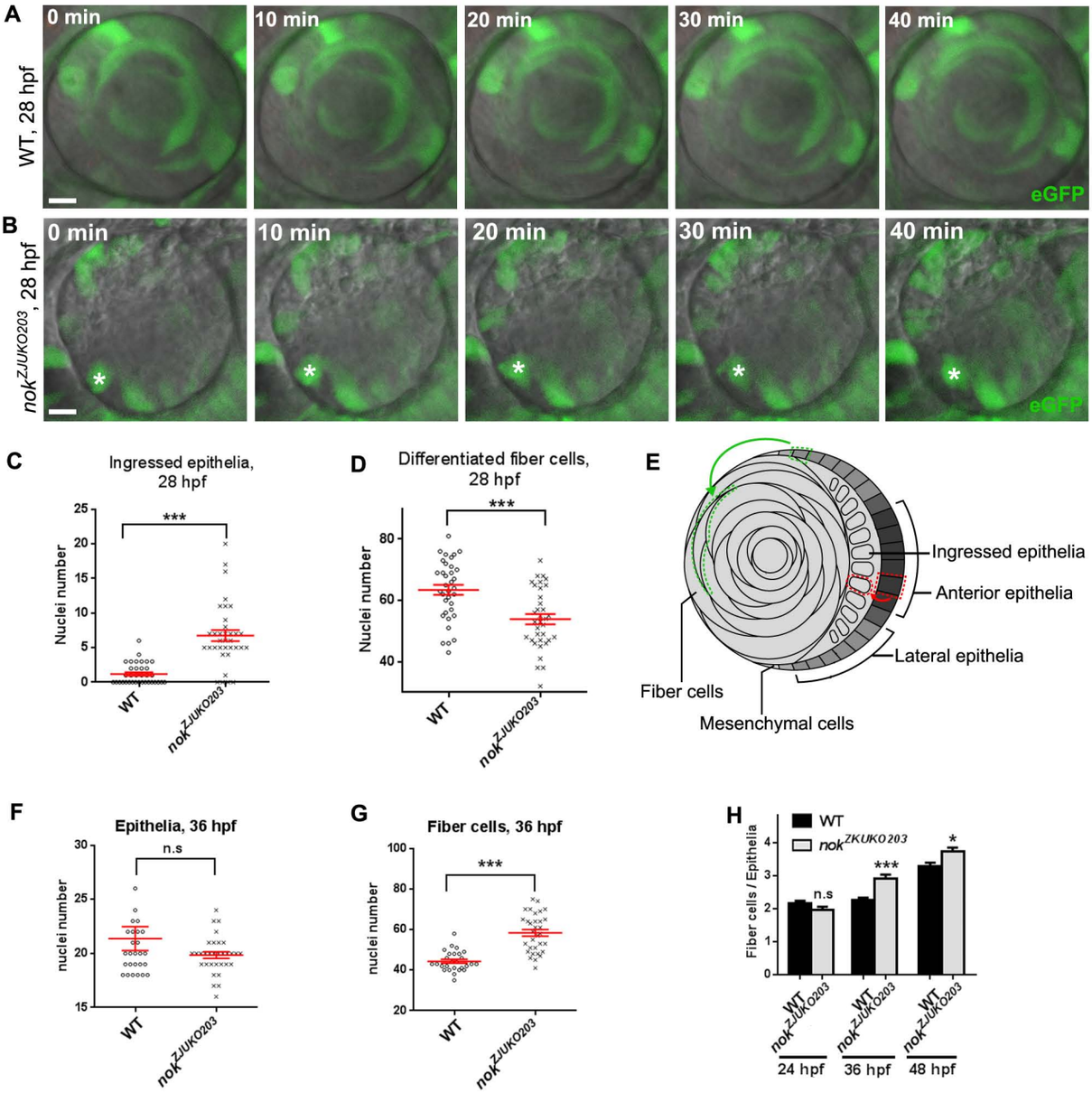

Figure S4. Depletion of Nok leads to invasive migration of epithelial cells in zebrafish lens.

(A and B) Lens epithelial cell migration in WT (A) and *nok* mutants (B) traced by time-lapse imaging. The lens epithelial cells in WT were stably positioned in the surface layer of the lens. A number of epithelial cells in *nok* mutants directly invaded into inner lens. * shows an invading epithelial cell in *nok* mutants.

(C and D) Quantification of cell number in inner lens at 28 hpf. C is the quantification of Zl1-immunoreactivity negative cells accumulated in inner lens in WT (e=1.2 ± 0.26) and *nok* mutants (e=6.74 ± 0.76). D is the quantification of differentiated fiber cells (Zl1-immunoreactivity positive cells) in inner lens in WT (e=63.43 ± 1.65) and *nok* mutants (e=53.89 ± 1.67). n = 35 embryos.

(E) Schematic illustration of lens cell migration. In WT, cells migrate into inner lens after epithelia-to- mesenchymal transition (shown by green arrow). In *nok* mutants, a quantity of epithelial cells invaded directly into inner lens (shown by red arrow).

(F and G) Quantification of lens epithelial cells and fiber cells number in 36 hpf WT and *nok* mutants. Lens epithelial cells number in WT (e=21.37 ± 1.1, n = 27 embryos) and *nok* mutants (e=19.84 ± 0.3, n = 32). Fiber cells number in WT (e=44.33 ± 0.95, n = 27 embryos) and *nok* mutants (e=58.31 ± 1.65, n = 32).

(H) Loss of Nok did not affect the ratio of fiber cells / epithelial cells at 24 hpf, but severely promoted the ratio at 36 hpf. The phenotype was alleviated at 48 hpf. n = 20 embryos.

*P<0.05, **P<0.01, ***P<0.001, n.s>0.05. Scale bar, 10 μm.

Figure S5

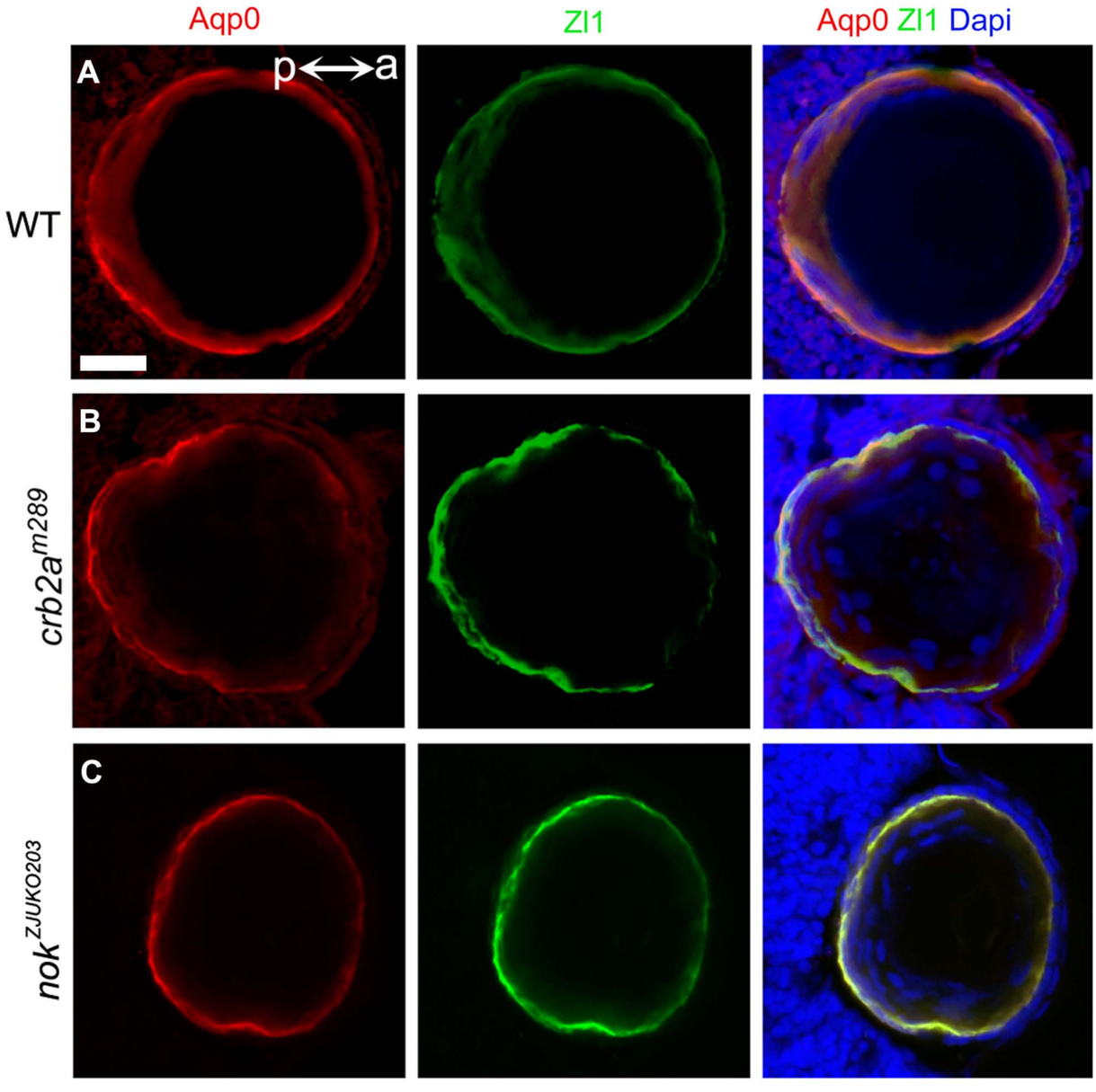

Figure S5. Loss of Nok did not affect the differentiation of lens fiber cells.

(A-C) Aqp0 and Zl1 staining in WT (A), *crb2a* (B), and *nok* mutants (C). Loss of Crb2a and Nok did not affect the differentiation of lens fiber cells at 72 hpf. Aqp0 (red) and Zl1 (green) are the markers of differentiated lens fiber cells (Imai et al., 2010; Korol et al., 2014). a (anterior) and p (posterior) in panel A show the lens orientation. Scale bar, 20 μm.

Figure S6

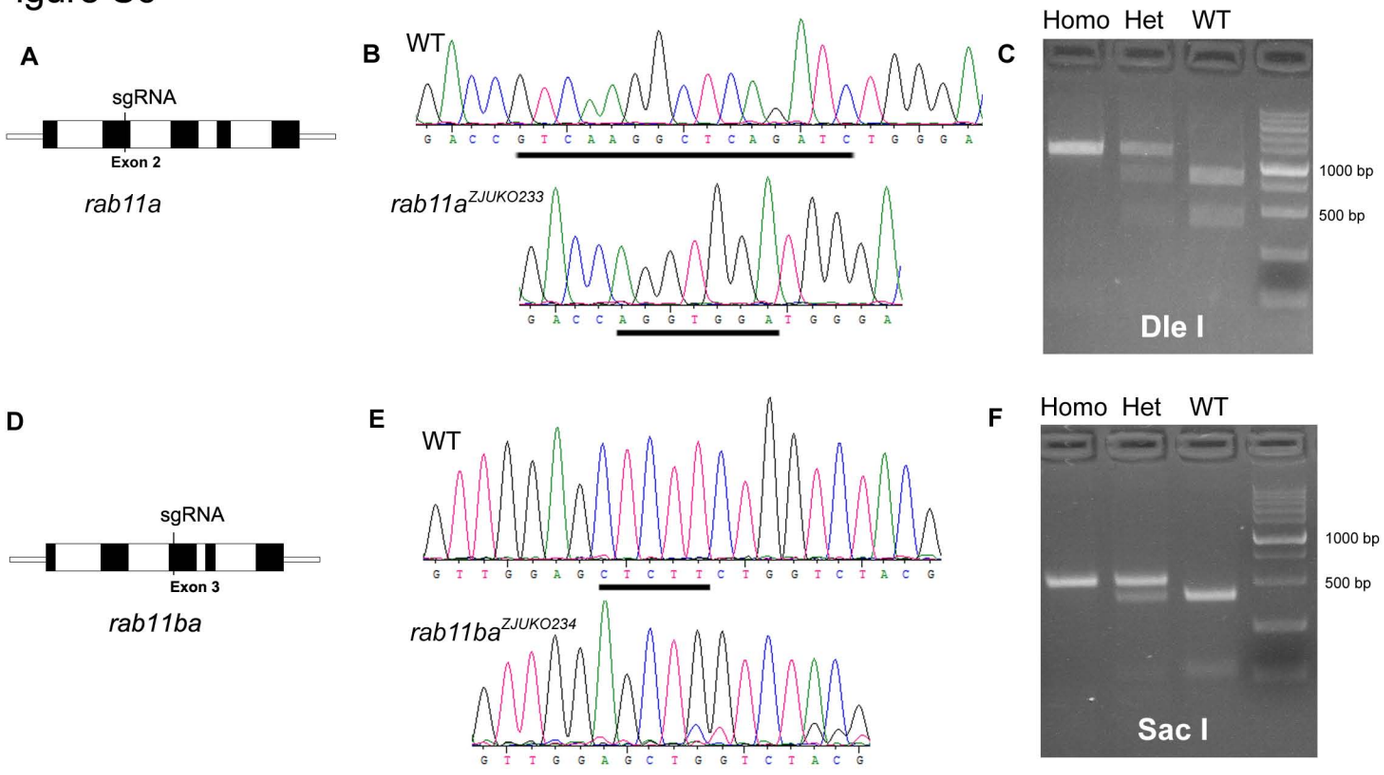

Figure S6. Generation of *rab11a* and *rab11ba* knockout zebrafish.

(A-C) A is the schematic illustration of the mutated position of *rab11a* gene. Sanger sequencing showed that 15 nucleotides were deleted and 7 nucleotides were inserted resulting in a truncated protein containing 88 amino acids (amino acid 1-59 of Rab11a and a 29 amino acids mistranslation) (B). The *rab11a*^{ZJUKO233} mutants were genotyped with PCR followed by digestion with restriction enzyme Dle I (C). a (anterior) and p (posterior) in panel A show the lens orientation.

(D-F) D is the schematic illustration of the mutated position of *rab11ba* gene. Sanger sequencing showed that 5 nucleotides were deleted, resulting in a truncated protein containing 112 amino acids (amino acid 1-92 of Rab11ba and a 20 amino acids mistranslation) (E). The *rab11ba*^{ZJUKO234} mutants were genotyped with PCR followed by digestion with restriction enzyme Sac I (F).

Figure S7

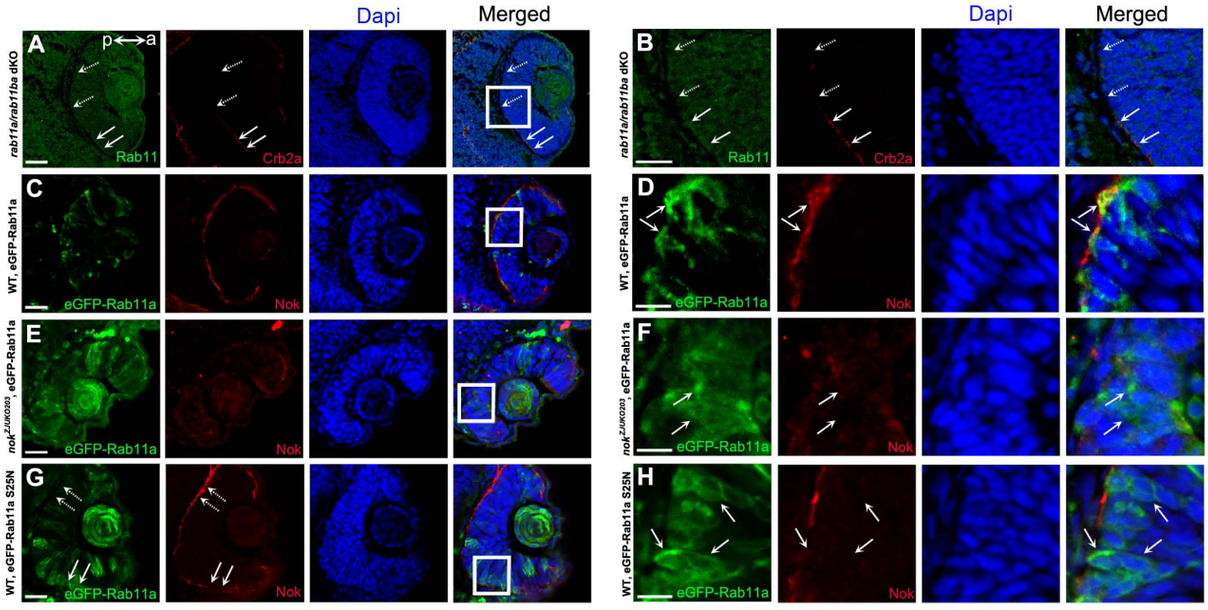

Figure S7. Apical localization of Nok and Rab11 are reciprocally dependent.

(A and B) The apical localization of Crb2a was severely disrupted in retinal neuroepithelial cells in *rab11a/rab11ba* dKO mutants. a (anterior) and p (posterior) in panel A show the lens orientation.

(C and D) eGFP-Rab11a enriched in the apical regions in retinal neuroepithelial cells in WT.

(E and F) eGFP-Rab11a was non-polarly distributed in retinal neuroepithelial cells in *nok* mutants.

(G and H) eGFP-Rab11a S25N was non-polarly distributed in WT retinal neuroepithelia, and impeded the apical enrichment of Nok.

Scale bar, 20 μm (A, C, E and G) and 10 μm (B, D, F and I). The embryos used in this figure were fixed at 36 hpf. B, D, F and H are the higher magnifications of the white boxed region in A, C, E and G respectively.

Figure S8

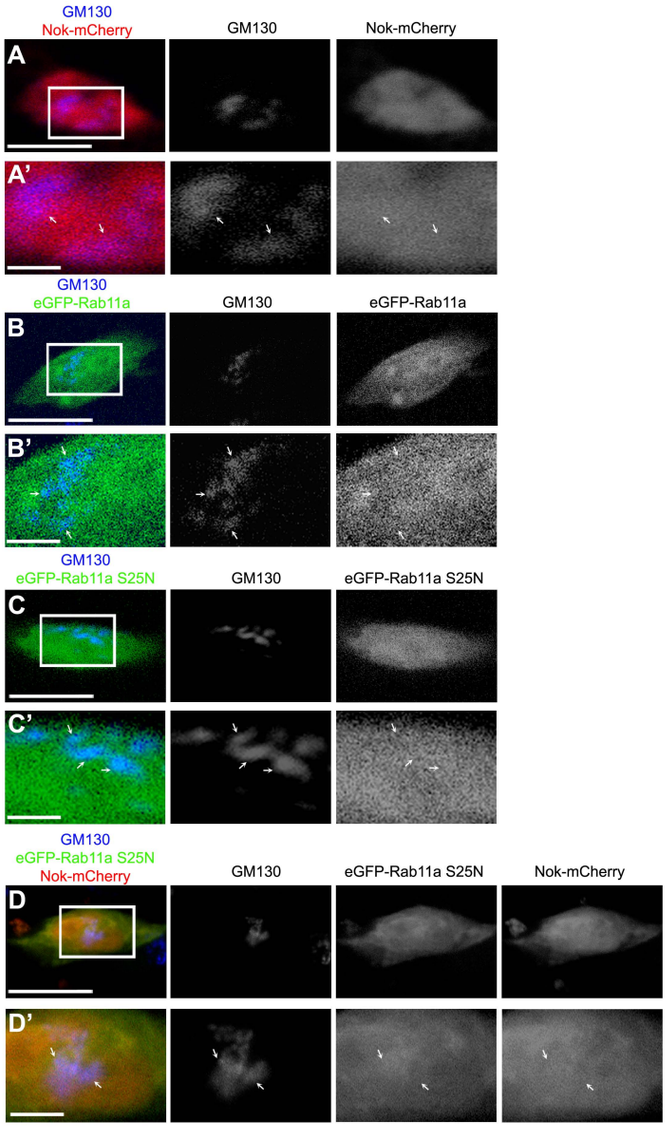

Figure S8. eGFP-Rab11a S25N did not aggregated in Golgi with Nok-mCherry in MDCK cells.

(A-C) Nok-mCherry (A), eGFP-Rab11a (B) and eGFP-Rab11a S25N (C) were spread in the whole cell without aggregation in Golgi when these proteins were individually expressed in MDCK cells.

(D) eGFP-Rab11a S25N and Nok-mCherry were spread in the whole cell without aggregation in Golgi when these two proteins were co-expressed in MDCK cells.

Arrows in A-D show the Gogli labeled by GM130. Scale bar, 10 μm (A, B, C, and D), and 2.5μm (A', B',C', and D').

Table S1, Oligonucleotides used for generating and genotyping the zebrafish knockout lines

nok^{ZJUKO203} sgRNA	GGATATGTGACCGAGTCAGATGG
rab11a^{ZJUKO233} sgRNA	GACCGTCAAGGCTCAGATCTGGG
rab11ba^{ZJUKO234} sgRNA	GGGTGCAGTTGGAGCTCTTC
nok^{ZJUKO203} genotyping forward primer	GTTACTATCTACAATGCTCTCCGGT
nok^{ZJUKO203} genotyping reverse primer	GTCTTCTGCGGTCCTCCTGCTGCTG
rab11a^{ZJUKO233} genotyping forward primer	GTTTGGAAAGACACAAGGCTTGAGT
rab11a^{ZJUKO233} genotyping reverse primer	GATCTTTGCTATGAACAGGCAGTTA
rab11ba^{ZJUKO234} genotyping forward primer	TAGGTTGTACAGCAATACAGATAAG
rab11ba^{ZJUKO234} genotyping reverse primer	CCACCAGCATGATGACGATGTTGTT

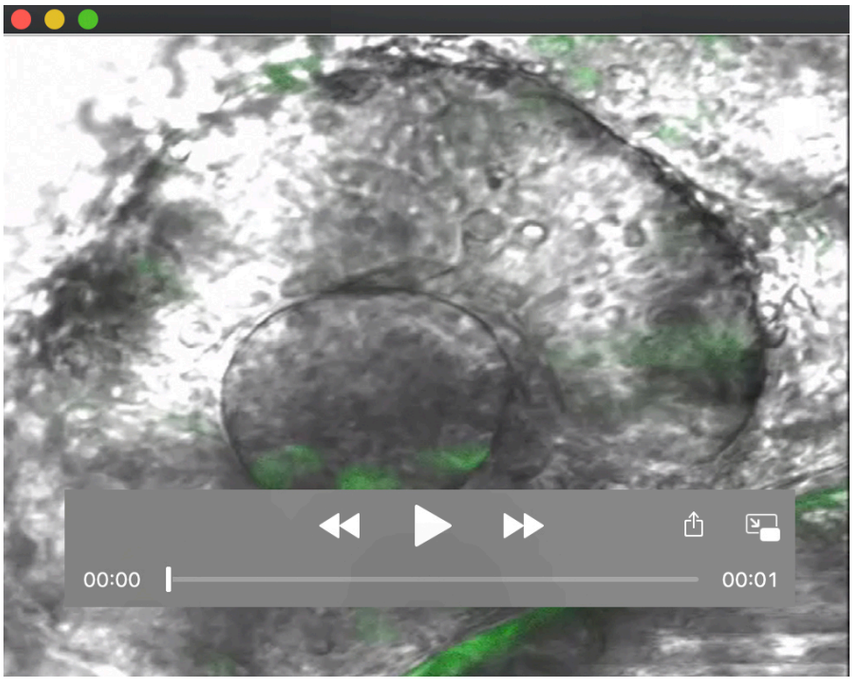

Movie 1. Time-lapse tracing of a WT lens. The lens epithelial cells in WT were stable in the surface layer of the lens.

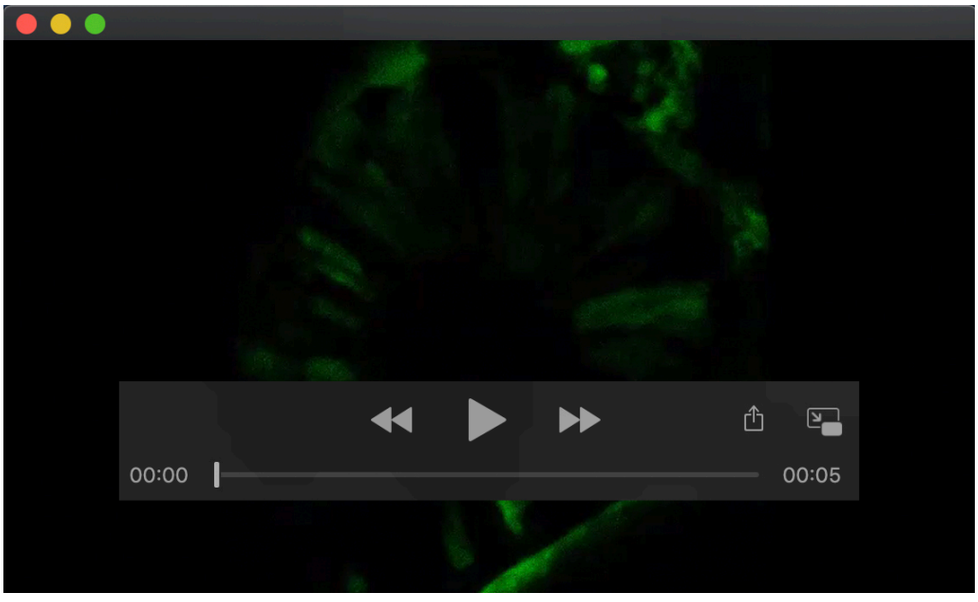

Movie 2. Time-lapse tracing of a WT lens. The same movie with movie 1 without the bright field image.

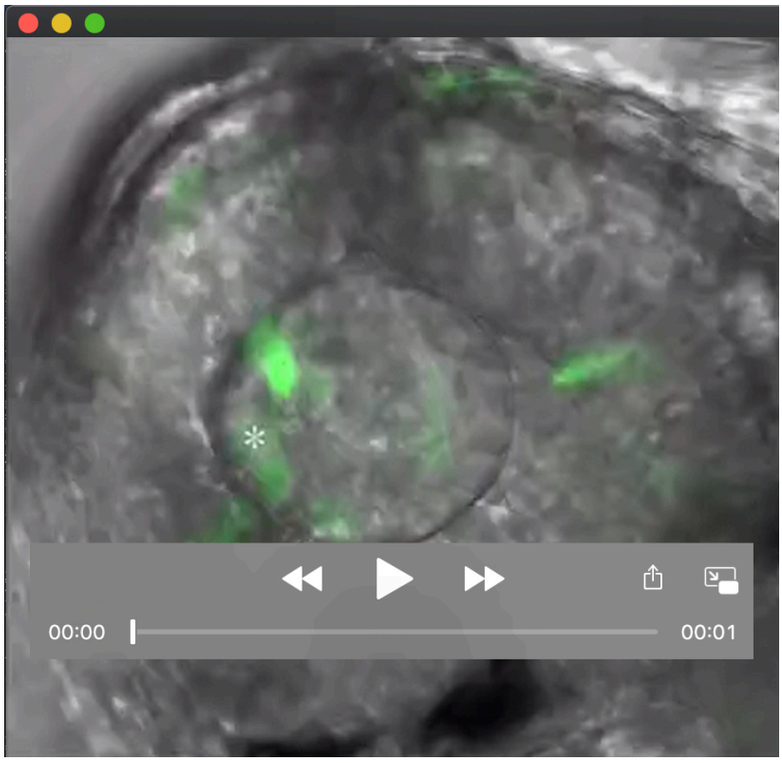

Movie 3. Time-lapse tracing of a *nok* mutant lens. The lens epithelium, which was marked by *, in *nok* mutant lens directly invaded into inner lens.

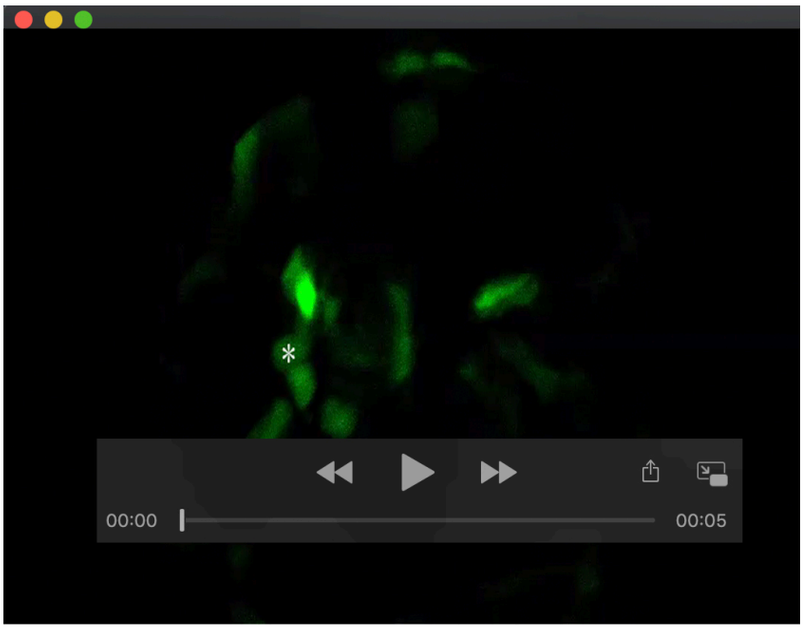

Movie 4. Time-lapse tracing of a *nok* mutant lens. The same movie with movie 3 without the bright field image.